SCIENTIFIC COMMITTEE
TWENTY-FIRST REGULAR SESSION

Nuku'alofa, Tonga
13 – 21 August 2025

Reference Model of Skipjack Tuna in the Pacific Ocean Using SEAPODYM Integrating Catch, Length, Tagging, and Early Life History Data

WCPFC-SC21-2025/SA-IP-20 (Rev.01)
17 July 2025

Inna Senina[1], Lucas Bonnin[1], Matthieu Lengaigne[2], Hidetada Kiyofuji[3], Kristine Buenafe[4], Dan Fuller[5], John Hampton[1], and Simon Nicol[1]

[1] Pacific Community. B.P. D5, 98848 Noumea Cedex, New Caledonia
[2] MARBEC, University of Montpellier, CNRS, IFREMER, IRD, Sete, France
[3] Highly Migratory Resources Division, Fisheries Stock Assessment Center, Fisheries Resources Institute, Japan Fisheries Research and Education Agency, Yokohama, Japan
[4] School of Earth and Environmental Sciences, The University of Queensland, St Lucia, QLD, 4067, Australia
[5] The Inter American Tropical Tuna Commission, La Jolla, USA

Contents

1 Executive Summary

1.1 Scope of work

This paper describes the updated reference model for the spatiotemporal dynamics of Pacific skipjack tuna, resulting from the integration of catch, length, tagging, and early-life history data for skipjack into the SEAPODYM model to inform its parameters.

1.2 Key Outcomes

This updated reference model for Pacific skipjack tuna relies on improved ocean forcing fields, enhanced spatial resolution, revised model structure, and newly available scientific data. It currently represents the most robust quantitative model for simulating the species' spatiotemporal dynamics.

Model validation shows improved predictive skill across all data types — catch, length frequency, tagging, and early-life history data — with statistical metrics outperforming those of the previous INTERIM model. Total biomass estimates in the Western and Central Pacific Ocean (WCPO) are partially consistent with the 2022 MFCL assessment, estimating higher biomass in regions characterized by warmest ocean, which the MLE approach identifies as the most suitable environment for skipjack.

The model analysis underscores the critical influence of interannual and decadal environmental variability on stock dynamics. Recruitment is primarily driven by ocean productivity in the western tropical Pacific, while zonal displacements of skipjack, as indicated by tagging and catch data, reflect the combined effects of ocean currents and active fish movement.

1.3 Report details

This report presents a detailed technical summary of the completed work, including updated parameter estimates and relevant model diagnostics. A comprehensive optimization using the full likelihood function was conducted to reduce potential biases from model parameters and forcing variables, and to obtain a maximum likelihood estimate (MLE) solution characterized by biologically realistic parameters. The resulting reference model demonstrates validity across independent datasets, offering robust predictions of stock dynamics with spatiotemporal structure that supports fishing pressure and well reproduces observed variability in the local catch rates.

An alternative parameterization — including a fixed Lorenzen natural mortality rate, as used in the current stock assessment model — was also estimated and compared to the reference model. Additionally, regional connectivity and the influence of ENSO-related variability on skipjack movement and recruitment were examined.

1.4 Main results

1. Informed by multiple sets of fisheries and scientific data over 1994-2012, a reference model provides valid predictions with estimated parameters on a 1° x 30 days resolution for the 1960-2022 period using JRA55-NEMO-PISCES hindcast with atmospheric reanalysis as forcing (Table 1).

2. In comparison to the previous reference model estimated with fisheries data and tagging data, the new solution exhibits more variable temporal dynamics linked to the inter-annual and inter-decadal variability of tuna environment (Figure 1). Predicted spatiotemporal dynamics of skipjack biomass density explains the high catches in the equatorial Pacific and observed zonal movements between warm pool and central Pacific related to ENSO variability (see Figures 28-29).

3. The total skipjack biomass in the WCPFC statistical area is estimated to be 7.1 million metric tons (Mt), based on the five-year average from 2018 to 2022 (Figure 1). The corresponding Pacific-wide biomass, including the Indo-Pacific region (100°E-70°W, 20°S-45°N) is 9 Mt, hence the EPO region contributing approximately 1.9 Mt. The fishing impact is evaluated for 2020 due to incomplete geo-referenced catches in 2021-2022 (see Figure 2). The stock reduction from virgin biomass is 26.5% for the WCPFC stock, 15.6% in the EPO region and 24% Pacific-wide.

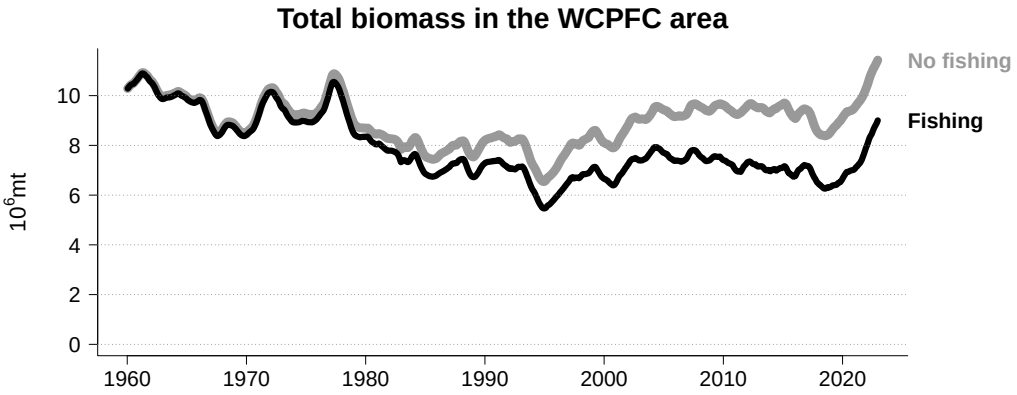

Figure 1: Total size of skipjack stock in the WCPFC statistical area (summed over stock assessment regions 1-8) predicted by SEAPODYM with the MLE parameters. The grey line shows the virgin (without fishing) biomass and the black lines show the biomass of exploited stock. Both curves are shown with monthly step.

4. Integration of early-life history data into the model and data likelihood improved observability of adult stock distribution, hence contributing to the estimation of movement rates. The fit metrics evaluated for independent catch and local catch rates, size frequencies samples, tagging and larval data are generally good and show improvement compared to the previous reference model (Figures 10-15).

5. This model produced a biomass distribution with a core area associated to the warm waters of the warm pool and central Pacific with splitting near the equator. In the eastern Pacific the highest densities of skipjack are predicted along the coasts of Central and South Americas, mainly in the zones of coastal upwelling and local productivity hotspots. e.g., Galapagos and NECC convergence zone. Seasonally, skipjack is predicted to migrate to the productive waters of Kuroshio Extension and Peruvian upwelling although these movements are still biased because of misrepresentation of ocean dynamics with 1° resolution (see Figure 19).

6. Although SEAPODYM estimates bigger stock of skipjack in the WCPO than MULTIFAN-CL (Castillo Jordán *et al.*, 2022), the estimates from two models are in agreement in terms of overall trends and recruitment levels for the period 1994–2019. The models diverge for earlier years: MULTIFAN-CL predicts an increasing trend in both recruitment and total biomass, whereas SEAPODYM indicates a decline in both estimates during that period (see Figures 24–25). The declining trend in SEAPODYM is primarily driven by the positive phase of the Inter-decadal Pacific Oscillation (IPO), which was characterized by reduced ocean productivity in the western Pacific Ocean. In contrast, the trend captured by MULTIFAN-CL is likely influenced by Japanese pole-and-line CPUE indices (Hamer *et al.*, 2024; Nishimoto *et al.*, 2024).

7. In terms of connectivity between assessment regions (see Figure 23), it was found that in the WCPO, the biomass is moving actively through the equatorial regions 6, 7 and 8 and only exchanges adult biomass with assessment region 4. The regions north of 10°N are interconnected and the net movement appears to be clockwise. Indo-Pacific region (assessment region 5) is found to be a biomass sink for adult skipjack, and a donor of skipjack larvae to adjacent Pacific regions.

8. The reference model indicates an eastward shift in the total skipjack biomass within WCPO, potentially linked to climate change (Figure 29). This finding will be further investigated using an ensemble of Earth System Model forcings.

1.5 Remaining Actions

9. Climate change simulations with reference model need to be completed with climate model outputs corrected from existing environmental forcings to provide an envelop of future projections.

10. Current reference model will also be re-estimated under the ERA5-NEMO-PISCES and JRA55-NEMO-PISCES with the latest PISCES parametrizations.

1.6 Acknowledgments

We thank Julien Temple-Boyer from Mercator Ocean International for data preprocessing and providing the micronekton fields. The continued development and application of the SEAPODYM model to the work of the WCPFC Scientific Committee is facilitated through Project 62. The project affiliates the independently funded work on SEAPODYM into the SC's work programme. It is conducted in collaboration with the Oceanic Fisheries Programme (OFP) of the Secretariat of the Pacific Community. Project 62 is currently supported by a Climate Change and tuna project coordinated by the Oceanic Fisheries Programme at SPC and FAO ABNJ2 Tuna Project funded by the Global Environmental Fund. The Inter American Tropical Tuna Commission has provided access to non-public domain data for the purposes of progressing the work programme of the WCPFC-SC.

2 Introduction

SEAPODYM is a model developed for investigating spatial tuna population dynamics, under the influence of both fishing and environmental effects. The underlying continuous equations of SEAPODYM are classical advection-diffusion-reaction equations with ageing term, describing the population dynamics in time, age and two-dimensional space. The population dynamics (spawning, movement, mortality) are constrained by environmental data (temperature, currents, primary production and dissolved oxygen concentration) and simulated distribution of mid-trophic (micronektonic tuna forage) functional groups. The model uses length and weight relationships obtained from independent studies. Different life stages are considered: larvae, juveniles and (immature and mature) adults. After juvenile phase, fish become autonomous, i.e., they have their own movement (linked to their size and habitat) in addition to be transported by oceanic currents. Fish are considered immature until pre-defined age at first maturity and mature after this age, i.e., contributing to the spawning biomass and with their displacements controlled by a seasonal switch between feeding and spawning habitat, effective outside of the equatorial region where changes in the gradient of day length is marked enough and above a threshold value. The last age class is a "plus class" where all oldest individuals are accumulated. The model includes a representation of fisheries and predicts total catch and size frequency of catch by fleet when fishing data (catch and effort) are available. The numerical model predicts the density of tuna population for each, generally monthly, age class. In addition to the full population model, SEAPODYM includes a model for tagged sub-population, which shares the same habitat and movement parameters. The observation models for catch, length frequency of catch, larval density, and tag recapture densities are predicting the observed quantities and a Maximum Likelihood Estimation approach is used to estimate model parameters.

The quantitative modelling of tuna population dynamics with SEAPODYM has been continuously improving, including development of reference models that integrate fisheries catch and length data for Pacific Ocean populations yellowfin and South Pacific albacore, and including also conventional tagging data for populations of skipjack and bigeye tunas (Senina *et al.*, 2019, 2020, 2021). Besides complete geo-referenced fisheries datasets for a given species, the 'new-generation' of SEAPODYM reference models include integration of tagging and early-life history data in the likelihood estimation approach, implementation of robust statistical methods for global sensitivity analysis and cost function profiling, enhanced algorithm of the fisheries data use within likelihood function and complete validation on independent data sets. This led to better estimates of both stock size and stock spatial structure.

This Information Paper presents the new reference model of Pacific skipjack tuna population (*Katsuwonus pelamis*), which primarily inhabits the tropical Pacific Ocean. The previous reference model constrained by fisheries and tagging data was presented in Senina *et al.* (2019). This study relies on the data from various tagging experiments conducted by SPC, FRA and IATTC between 1979 and 2022. The integration of tagging data allowed better estimation of habitat indices parameters and movement rates, and the integration of larval data constrained the spatial distribution and seasonality of skipjack larvae and allowed better observing the adult spawning stock. The estimation of all model parameters was performed in the optimization experiments for the whole Pacific Ocean

and 22-years long (1991-2012) period representing the most complete data coverage. The fishing data and fisheries definition have been carefully revised before running this new model configuration.

Here we report the main results from updated reference model and demonstrate how integrating scientific data (tagging, laboratory studies, field larval sampling) influences the model parameters and allows improving model consistency with the data. We present the results of the optimization study performed with the full-likelihood, CLTE, model. Finally we evaluate the fit and validate the CLTE model using catch, length, tagging and larval data. To do so, we use only independent data. The results of this study are discussed, highlighting both the improvement and deficiencies and suggesting the next steps aimed at improving the new reference model.

The aim of the current study was to update the previous quantitative reference model for Pacific-wide skipjack tuna population (Senina *et al.*, 2019) using better environmental forcings, higher 1-degree resolution, all available geo-referenced fisheries data, historical conventional tagging data, and scientific data on early-life history of skipjack to enable less biased and higher resolution climate projections.

3 Data

3.1 Environmental data

The forcing configuration of the current SEAPODYM application is summarized in Table 1. Forcing variables were generated by the coupled ocean-biogeochemical model NEMO-PISCES forced by the atmospheric reanalysis JRA-55. The Japanese 55-year Reanalysis (JRA-55) is a comprehensive atmospheric reanalysis dataset developed by the Japan Meteorological Agency (JMA), covering the period from 1958 to February 2024. NEMO-PISCES refers to the coupling of the NEMO (Nucleus for European Modelling of the Ocean) physical ocean model with PISCES (Pelagic Interactions Scheme for Carbon and Ecosystem Studies), a biogeochemical model developed to simulate the oceanic carbon cycle and lower trophic-level ecosystem dynamics. NEMO provided the physical environment — ocean currents and temperature — while PISCES supplied primary production data and estimates of the euphotic layer depth. Together, the NEMO-PISCES system forced by an atmospheric reanalyses enables realistic simulations of ocean variables in hindcast mode. This hindcast simulation, hereafter JRA55, was prepared by the French Institute of Research for the Development over 1958-2022. It has horizontal resolution of 1° in the temperate zones with a refined resolution of 1/3° in the equatorial band (ORCA1 grid). The JRA55 model outputs have been interpolated to a regular grids of 1°, the domain boundaries were defined by the land mask, which is built from both global bathymetry data (ETOPO1, https://www.ngdc.noaa.gov, doi:10.7289/V5C8276M) and physical data availability in the coastal grid cells. Finally, the mid-trophic level (micronekton) biomass fields were simulated on a regular grid and monthly time step by the SEAPODYM-LMTL model. The interpolated ocean forcings and the outputs of the micronekton model were prepared by Mercator Ocean International (https://www.mercator-ocean.eu).

3.2 Skipjack tuna fisheries

The industrial fishing fleets targeting skipjack tuna comprise mainly two fishing gears - purse seine and pole-and-line (see e.g., Pacific Community, 2022) with the majority of catches coming from purse-seine fleets in WCPO. There are also a few accidental long-line catches of skipjack. Total annual catches by gear being used in the current SEAPODYM model are shown in Figure 2. It is important to have the complete geo-referenced dataset that corresponds to the total landings in terms of total annual removal from the stock in order to correctly take into account the mortality due to fishing. Some discrepancies exist between WCPO purse-seine catch data (Figure 2), but these missing records are not available in a geo-referenced format. Their absence represents an underestimation of total fishing mortality, but likely does not have significant impact on the estimation of model parameters.

Skipjack tuna geo-referenced fishing data are provided by SPC and IATTC (Figure 3). Each fishery in SEAPODYM is defined by a single selectivity function and a catchability coefficient that may be allowed to increase/decrease linearly with time. Once the fisherman-driven causes of changes in catchability, such as changes of target species or the fishing strategy are removed from the fisheries, we assume that the remaining variability in catchability is driven by the spatial distribution associated with the environmental variability and fish movements, which are explicitly described by the model. Therefore it is critical to have a definition of homogeneous fisheries in terms of constant in space and time catchability and selectivity coefficients (Forestier *et al.*, 2025). The definition of fisheries for Pacific skipjack tuna, which is assumed to satisfy to such criterion is provided in Table 2.

Size frequency data have variable resolutions ranging from 1° x 1° to 10° x 20°. Temporal data coverage is shown in Figure 4. In the EPO the size data are provided for purse-seine fleets over IATTC sampling regions (see e.g. IATTC, 2010), however available data set spans until year 2012 and the update was not received for this study for technical reasons. This limited the time period for parameter estimation with fishing data. Note also, that catches by Japanese fisheries north of 35°N were excluded from the datasets due to existing biases in the ocean forcings (southern shift of Kuroshio currents extension in 1° resolution) and potentially in the vertical structure of SEAPODYM, which prevent the model from predicting high skipjack densities at these latitudes.

3.3 Conventional tagging data

The conventional tagging campaigns in the Pacific Ocean were conducted extensively since 1960s by major regional fisheries organizations such as WCPFC/SPC and IATTC, and Japanese Fisheries Research Agency (FRA). In particular, SPC has conducted several large tagging experiments, releasing several hundred thousand tagged fish since the 1980's in the western and central Pacific region. Since 2008 alone, SPC has deployed 199,075 conventional tags on skipjack tuna in the WCPO (see Figure 5). IATTC and the FRA have been also very active in tuna tagging, in the eastern and north-west Pacific, respectively. FRA have been aiming at capturing movement of skipjack between the tropical zone and Kuroshio current extension. In combination, these data provide key information on movement and mortality of the stocks at a Pacific-basin scale and for exploring skipjack movements and mixing across different oceanic regions (Scutt Phillips *et al.*, 2022).

Tagged skipjack tuna are recaptured by fisheries after time at liberty between a several days to several years. For example, since late seventies, a quarter of all recaptures stayed less than 30 days at liberty, with maximum about 4 years in WCPO and 3 years in EPO (Figure 5). The rate of recapture for skipjack tuna in the tropical WCPO typically varies between 10-25%, but can reach as much as 50% in the closed habitats such as Bismarck Sea. In the EPO, the recapture rate is smaller, about 7-12%. Observed lengths of skipjack cover the largest portion of juvenile and adult population in the WCPO, and mainly adult tuna in the EPO, with significantly higher (compared to WCPO) contribution of larger tuna of 60-70 cm caught by the purse-seine gear in this region (Figure 5).

Conventional tagging data are integrated into the optimization method in SEAPODYM to inform habitat and movement parameters. Only recapture-conditioned data are used in the model (see the Method section). Besides, a sub-set of tagging data is used to inform model parameters, while the remaining data are reserved for validating the MLE solutions. The important reason to choosing the control subset is the reduction of the computational cost, that depends on the number of the tag groups whose movement must be numerically resolved. The temporal coverage and distribution — in terms of mean length and time at liberty — of the tagging data subset selected for optimizations are illustrated in the Figure 5.

3.4 Early-life history data

Two types of early-life history data were used in the current reference model development. First, we used the results of an experimental study conducted in Japan at the Kagoshima City Aquarium with skipjack tuna reared in captivity and observed by researchers during natural spawning and immediate egg development under precisely controlled thermal conditions (Fujioka et al., 2024). Optimal temperature range for hatching success was found to be between 23°C and 31°C, with hatching rates exceeding 50% across this range. Highest hatching rates occurred around 27–29°C. At extreme temperatures (21°C and 33°C), no eggs survived. Hatching duration decreased with rising temperature, from about 37 hours at 22°C to about 16 hours at 32°C. A shorter hatching time at higher temperatures reduces exposure to predators, offering an ecological advantage. The relationship between temperature and hatching success established in this study can be seen in Figure 6. The upper temperature limit for viable hatching is newly extended to 31°C, which is higher than previously reported in earlier studies using artificial fertilization. These findings were directly incorporated into the skipjack model of early larvae (see Model section).

Another source of early life history data comes from larval sampling surveys conducted using plankton nets by Fisheries Agency of Japan Far Seas Fisheries Research Laboratory from 1956 to 1981 (Nishikawa *et al.*, 1985; Davis and Nishikawa, 1989), which provided estimates of larval catch-per-unit-effort (CPUE) at 1° spatial resolution. While these surveys offer insights into local larval densities, the available datasets are published or digitized in aggregated, categorical formats, which limits their direct utility for parameterizing models (Bonnin and Senina, 2024). As an alternative, derived products — such as spawning habitat indices estimated from the original survey data using geostatistical models (Ijima and Yusup, pers. comm.) or outputs from boosted regression tree models — can be incorporated into the model likelihood. In the present study, we relied on the latter approach (see Figure 6).

4 Model

4.1 SEAPODYM.v5

Since the development of the previous reference model, the SEAPODYM code has undergone several improvements and major changes, significantly impacting the workflow and enhancing the MLE solution for skipjack. The current reference model uses an updated version of SEAPODYM (v5.1). The main code changes and model improvements are outlined below.

- A cleaner and better structured public codebase on GitHub (https://github.com/PacificCommunity/seapodym-codebase.git), which compiles into five different binaries *seapodym* for simulation runs, *seapodym_clte* for simulation and estimation, *seapodym_densities* with estimation model for unexploited stocks, *seapodym_habitats* for habitat models with parameter estimation, and *seapodym_fluxes* to compute regional connectivity in the population dynamics model with or without fishing.

- Integration of early-life history data including eggs hatching success as a result of laboratory studies, larval density from broad scale larval surveys, and spawning seasonality from adult gonad sampling studies.

- More flexible set-up of tagging data to inform movement parameters, including minimal density threshold for the inclusion of tag recapture groups and selection of tags by time at liberty.

- Changes in the model structure such as new observation model for early larvae observed in larval net sampling, alternative models for reproduction, accessibility to vertical layers, diffusion and mortality, and normalization of parametric prey function of spawning habitat to enable unbiased reproduction rate estimation.

- Changes in parameter estimation implementation including i) a decrease the RAM needs by 55%, ii) Taylor derivative test, iii) arbitrary number of forage groups in the estimation model, iv) estimation of catchability trend parameter, and v) stock likelihood term as a penalty function.

4.2 Model structure

The model PDE equations and the functional links between species habitats and environmental drivers are fully described in SEAPODYM Reference Manual (2022). Given that tropical skipjack tuna is known to be an opportunistic spawner and does not undertake long-distance spawning migrations, seasonal spawning migrations were disabled in the model. As a result, the modelled skipjack spawns whenever feeding habitat conditions are also favorable for spawning.

Six different life stages are considered in current modelling: eggs (result of adults' spawning), early larvae (0-7 days old), larvae (7 days to 1 month old), small juveniles (1-3 months old), juveniles (older than 3 months but not yet reached age of 50% maturity, which is set to 11 months), and adults, including only a mature part of the population ($>$ 11 months old corresponding to fork length $>$ 43.7cm). Note, in terms of movement

modelling, only two stages are differentiated based on their vertical and horizontal movement behaviours: larvae and small juveniles drift with epipelagic layer currents while their survival depends on spawning and juvenile habitat conditions respectively; juveniles and adults move passively with currents within their preferred vertical layers and move actively along feeding habitat gradients.

The fisheries mortality was computed using both methods: using fishing effort according to Gordon-Schaefer model, or using catch removal method (Senina *et al.*, 2019; SEAPODYM Reference Manual, 2022), applied to the fisheries according to their data quality and target species properties (Table 2).

The early larvae model is the new observation model that was introduced in SEAPODYM.v5 to enable direct comparison of model predictions with the larval survey observations. Specifically, this model component was designed to predict the density of larvae within the size range typically captured by plankton nets used in Japanese surveys (Nishikawa *et al.*, 1985), where the average size of larvae was around 4 mm and larvae larger than 7 mm are rare (Davis and Nishikawa, 1989; Strasburg, 1960). Taking into account the typical size of newly hatched larvae (2-3 mm) (Matsumoto and Walters, 1958) and their rapid growth during the early development, for example, yellowfin larvae exceed 12 mm just after five days of feeding in tanks (Scholey *et al.*, 2012), the larvae observed in these surveys are likely only a few days old, having just completed the first two developmental phases: the egg and yolk-sac phases. So, the method consists in splitting the first month of life into two distinct periods, each modelling separately with different habitat preferences and hence different mortality rates. At time zero, the density of eggs is described using the Beverton-Holt function as a result of spawning by adults. During the first time period, the dynamics of eggs and early larvae are modelled using advection-diffusion-reaction equation (ADRE) with passive transport by currents and mortality rate dependent solely on water temperature. Because the duration of the first two larval development phases is temperature-dependent, we set a maximum duration of seven days to fully capture development up to the sizes observed in surveys. After the first week all larvae have entered the autonomous phase of development and become dependent on food, hence larval dynamics are simulated using the default model configuration, that is, with ADRE incorporating passive drift and a mortality rate driven by the spawning habitat, which accounts for temperature, prey availability, and predator presence. This phase is modelled over the remainder of the 30-day time step, i.e., the following 23 days.

Also, since the early larvae model covers two distinct development phases, two temperature functions are considered: one for egg phase that is fitted to the relationship between hatching success and temperature established in experimental study by Fujioka *et al.* (2024), and another for yolk-sac larval phase from the spawning habitat model. Preliminary tests adding a prey-dependent function based on phytoplankton to account for the onset of the feeding phase during the first week of development showed to have no impact on the results, so the simpler model was retained for now. The final formula for early mortality rate used in the model of early larvae is the following:

$$M_0 = 0.5 + 3.38\left(1 - f_1 \cdot \left((1 + 0.24^{T_0 - 21.83})^{-1} + (1 + 0.19^{32.6 - T_0})^{-1} - 1\right)\right) \qquad (1)$$

where T_0 denotes SST, $f_1(T_0; {T_0}^*, \sigma_0)$ is the thermal preference function of the SEAPODYM spawning habitat, and a constant 0.5 is a reasonable, but still arbitrary value of early mor-

tality, which does not depend on environment. Since we do not have the larval abundance data, and because this parameter is by definition highly correlated with reproduction coefficient, its effect on the overall result is negligible. The results of the calibration of egg survival and of the early-life survival given by Eq. 1 are shown in Figure 6 (grey and blue lines).

4.3 Static model parameters

The estimates of length-at-age, weight-at-age and maturity-at-age relationships were taken from the 2016 MULTIFAN-CL assessment report (McKechnie *et al.*, 2016) and interpolated to the model age structure (Figure 7). One more model parameter, the maximal predation mortality at age 0, is systematically set to constant in the optimization experiments due to high correlation with the reproduction rate R of the Beverton-Holt function. In addition, all parameters of Eq. 1 were fixed, even the function f_1 parameters, which were fixed to values obtained while fitting spawning habitat only to the BRTM outputs using seapodym_habitats application.

4.4 Numerical configuration

The model PDE equations (SEAPODYM Reference Manual, 2022) were numerically solved with a monthly time step and two spatial resolutions, on a 1° and 2° regular grids covering the spatial domain of the Pacific Ocean $\Omega = \{x \in (100°E, 70°W), y \in (59°S, 61°N)\}$. Neumann boundary conditions were used in all runs. Besides, the buffer zone was specified in the Indo-Pacific region to limit the reproduction and biomass exchange with this region in order to avoid biomass accumulation due to closed boundary at $100°E$. The final predictions with estimated parameters were then done on the Indian and Pacific oceans domain, without the buffer zone, $\Omega = \{x \in (30°E, 70°W), y \in (59°S, 61°N)\}$.

The age between 0 and $a_{max} = 3$ years is discretized into monthly age classes and 2 more years are modelled as a single A+ class, thus resulting for skipjack in 37 age classes covering five years of life span.

During the first set of optimisation runs the estimated state of the INTERIM model (Senina *et al.*, 2019) was used as the initial conditions. Furthermore, the predictions of the first four years of simulation were not included into the likelihood to reduce the effect of the initial conditions on the MLE solution.

5 Methods

5.1 Integration of conventional tagging data

The method of integrating recapture-conditioned tagging data is described in Senina *et al.* (2019) and SEAPODYM Reference Manual (2022). The measurement model for tag recaptures describes the observed density of tagged individuals only. Thus, re-defining the state variable of the advection-diffusion-reaction model used in SEAPODYM, as the density of tagged fish at observed ages, varying in time at spatial location, we can design the tag estimation model. Since the objective of integrating tags is to inform movement

and habitat parameters, we use only recapture-conditioned tags. Thus the state variable represents the density of a group of tagged fish, which were released at different times and locations, and all recaptured at the same time at different locations. The solution of such PDE equation at the known time of recapture of a given group of tags is the density of recaptures, which is then compared to observed density of recaptures. Solving these PDEs for each group in four dimensions and with the same movement parameters as the full population model, and optimizing the tagging data likelihood together with other likelihoods, we estimate habitat and movement parameters. Obviously, an assumption has to be made is that the movement of tagged fish obeys the same physical principles as of untagged population and is led by the same environmental drivers that control the movement of all fish in the population.

An important advantage of this approach is that it accounts precisely for the time at liberty of all tags, which is otherwise impossible as the modelled quantity cannot be traced in the Eulerian model. Second, using only recapture-conditioned observation allows removing uncertainty related to the use of reporting rates and fishing effort to predict the tag recapture. However, there are still some caveats to consider while integrating individual movement data into a Eulerian model, which is not designed to predict the displacement of individual fish. One needs to have enough individual data to make an assumption on validity of a Eulerian model, which is suitable to describe movement of a large number of individuals. It is therefore important to select the time period with massive release-recapture data, providing hundreds of tag recaptures for each model time step. Also, to account for an uncertainty associated with the recapture position, and to transform the individual data to fish density, a bivariate Gaussian kernel for two independent variables (longitudinal and latitudinal coordinates) is applied to the observed recapture records. Also, in the observation model, the tags are aggregated into coarser spatiotemporal strata, here 2 degree spatial resolution and 3 months temporally. Finally, the tags which were recaptured in less than 10 days were excluded from likelihood because of the monthly stepping of the numerical model. It corresponds to removal of 15% records from the observational dataset.

In the current model configuration, we used 46 tag groups comprising a total of 12,974 tags, the majority of which were released and recaptured in the equatorial Pacific during the 2009–2011 tagging campaign. An additional 254 tags were released earlier by the Japanese Fisheries Research Institute between 1994 and 1999 to study skipjack feeding migrations toward the Kuroshio Extension (Figure 5). Although limited in number, these tags were assumed to be representative of typical migration routes in the region, which are influenced by external forces such as the Kuroshio currents. The remaining tagging data, covering the period from 1979 to 2022 and comprising 19,688 tags, were reserved for model validation.

5.2 Integration of early-life history data

The methods of integrating the early-life history data is fully described in Bonnin and Senina (2024). The seasonally averaged data are integrated into the data likelihoods. For categorical data, such as digitized larval densities (Buenafe *et al.*, 2022), the categorical equivalents of Poisson, Zero-Inflated Poisson, Negative Binomial and Zero-Inflated Negative Binomial likelihood functions were implemented and tested using the identical

twin experiments approach. In twin experiments, the model outputs are fitted to the pseudo-observations, which are sampled from model solutions given the spatiotemporal distributions of observed datasets. This technique provides valuable insights into observability of model parameters and performance of optimization method. It was shown that with categorical data, optimal spawning habitat parameters could not be re-estimated, irrespective of data quantity and spatial distribution. Hence the categorical nature of larval CPUE data (Nishikawa *et al.*, 1985) poses a limitation for its use in parameter estimation. In contrast, using continuous data, such as derived from the categorical inputs through boosted regression tree models (BRTMs) developed by Buenafe *et al.* (2025), has proven to be a successful approach.

To predict habitat suitability, which are the outputs of BRTMs, early larvae densities were computed by early larvae ADR model (as described in section 4.2) over the first week of species life. These densities were then averaged into seasonal distributions and multiplied by a linear scaling parameter, which was included as an additional variable parameter in the MLE approach. This mapping assumes that the BRTM outputs scale linearly with the observed larval CPUE, representing a simplification. In further developments, and in the absence of continuous larval data, we plan to explore alternative non-linear relationships between aggregated larval densities and habitat suitability indices. In particular, we aim to investigate how this simplification may affect the estimation of the density-dependence parameter in the Beverton-Holt function.

5.3 Maximum likelihood estimation

The MLE approach used in SEAPODYM is fully detailed in SEAPODYM Reference Manual (2022). In this reference model, the log-negative likelihood function, denoted as $L^- = -ln(L)$ to be minimized consists of four terms $L^- = L_C^- + L_{LF}^- + L_T^- + L_E^- + \beta$, where the likelihood terms describing the contribution of each dataset are defined differently. As in the previous skipjack application (Senina *et al.*, 2019), the catch data likelihood $L_C\left(\boldsymbol{\theta}|C^{obs}\right)$ was chosen to follow Poisson distribution for all fisheries with Gordon-Schaefer catch prediction method (depending on the fishing effort), and the normal distribution for all fisheries with catch removal method. The length-frequency of catch likelihoods $L_{LF}\left(\boldsymbol{\theta}|Q^{obs}\right)$, with Q^{obs} being the relative observed length frequency, were set to follow robustified normal likelihood for all fisheries (Hampton and Fournier, 2001). The tag recapture density likelihood, $L_T\left(\boldsymbol{\theta}|R^{obs}\right)$, and the BRTM outputs for larval suitability index, $L_E\left(\boldsymbol{\theta}|I_{EL}^{brtm}\right)$, were chosen to follow normal distribution. Finally, additional stock quadratic penalty function does not allow the mean stock biomass over region $(120E, 70W, 20S, 45N)$ to exceed 8.5Mt.

5.4 Optimisation runs

The selection of the time period for parameter estimation was guided by data availability. The lower bound was set to the early 1990s to coincide with the expansion of purse-seine fisheries and the availability of reliable catch, length and massive tagging data (see Figs. 2, 4 and 5). The upper bound was set to 2012 due to the availability of length frequency data in the Eastern Pacific Ocean (EPO). The first four years of model predictions were excluded from the catch and length likelihood calculations. As a result, in the optimization

runs, the model span over 1991-2012, and the data likelihoods were evaluated for the following years: catch and length frequency likelihoods over 1995-2012, tag recapture likelihoods over 1994-2012, and early larvae likelihood using the seasonal averages over 1995-2000.

As in the previous skipjack model, the purse-seine catches were computed without fishing effort in all optimization experiments. The Japanese pole-and-line fishery P23 was assumed to have constant catchability and selectivity during the optimization period. Note also that some fisheries (Table 2) were not used in parameter estimation due to being outside of the time interval for maximum likelihood estimation (P21, P22), or a valid spatial domain (O9 in the buffer zone, effort and catches north of 35°N due to ocean current bias). Two small fisheries, S13 and P14, were also added for validation only.

Extensive optimization study was carried out to explore the MLE sensitivity to fisheries structures, model structure setup and choice of variable parameters and their initial and boundary values. In addition, the new type of early-life observational data, were first used with the spawning habitat model to investigate whether the SEAPODYM spawning habitat index describes the habitat suitability modelled with BRTMs from categorical larval CPUE (Buenafe *et al.*, 2025). The majority of optimization runs were performed at a spatial-temporal resolution of 2° x 30 days, using degraded ocean forcing fields. This reduced-resolution setup preserves the essential ocean dynamics while significantly reducing computational cost. The configuration comprising model structure, observational dataset structure, and a selection of variable parameters that yielded the best maximum likelihood estimate was subsequently used for final optimizations at higher resolution (1° x 30 days), i.e., with the original, full-resolution ocean forcing.

5.5 Model validation

To conclude whether the obtained solution of the optimisation problem provides the best parametrisation given the model structure, the ocean forcing and the observational datasets, each optimisation run has to be analysed and validated. First, the quality of the fit to the data being used in the minimization, is evaluated. This is done with help of statistical metrics, which are selected depending on the type of the data: i) the R-squared goodness of fit, measuring how much the model is a better predictor to the data than the mean of the data; ii) the squared Pearson correlation coefficient, measuring the proportion of the variation in data described (explained) by the model iii) the root-mean-squared-error (RMSE) and the normalized mean-squared-error (NMSE); iv) residual variance and temporal bias; v) relative error; vi) model to data variance ratio. Fit to the size frequencies is evaluated with two metrics, normalized root-mean-squared-error (NRMSE) and standardized bias, the first indicating how well the shape of the frequency distribution is reproduced and the second one indicating how far off the model's predicted mean is in terms of the variability of the observed data.

Second, the parameter estimates are examined and confronted with the existing knowledge on the modelled species. Some important biological characteristics, such as thermal preferences, spawning sites and seasonality, and the species life span are reported in scientific literature. Finally, the model is systematically validated using independent sets of fisheries and tagging data, i.e., the data not used in the likelihood calculations. The same statistical metrics are computed for these independent datasets and compared to

the original fit metrics obtained with MLE data. For larval data, since it is represented by seasonal means, model fits can be assessed across different time periods and validated using the period that corresponds to the observations (Nishikawa *et al.*, 1985). This validation is carried out by calculating correlation coefficients for seasonal variations in regional larval densities and by comparing the larval counts within ranges of environmental variables: sea surface temperature (SST), primary production, dissolved oxygen and epipelagic micronekton.

6 Results

Model parameters described in this section were estimated from catch, length, conventional tagging, and climatological early-life history data (Buenafe *et al.*, 2025). Observing the modelled processes through all model dimensions in the optimizations, allowed estimation of main dynamic parameters, driving recruitment, mortality, habitat indices and movement rates. They were first estimated with the SEAPODYM model numerically resolved on a 2° x 30 days, then re-estimated with the same overall configuration, by changing only a spatial resolution of the model to 1° and selecting the best solution from jitter runs.

6.1 Optimal parameters

This section describes the maximum likelihood estimates of model parameters related to the population dynamics and their role in the key dynamic processes: reproduction, survival, and movement. All SEAPODYM parameters defining the reference model of skipjack tuna, both fixed and estimated, are provided in Table 3. This table includes also the MLEs obtained with fixed Lorenzen mortality.

6.1.1 Spawning habitat and reproduction

Incorporating recent findings on thermal conditions for eggs survival into the model changed how skipjack larvae survival is described. In the current model, the spawning habitat no longer influences the distributions of larvae at age zero. Instead, the effect of temperature on eggs survival is fixed, based on the experimental results from by Fujioka *et al.* (2024) (See Figure 6), and the spawning habitat index now only affects the mortality of larvae during the active feeding phase. In both configurations, the spawning habitat parameters and functional relationships with environmental variables are estimated to be similar (Figure 8). The thermal Gaussian function of the spawning habitat is estimated to have very large standard deviation and the mean centred at high temperatures, which do not occur in the open ocean. This implies that larval mortality increases with decreasing sea surface temperature, without a temperature interval where mortality is minimal (i.e., reduced to the fixed predation mortality rate). Both models show a strong dependence of larval survival on prey availability (represented by primary production linearly converted to phytoplankton wet weight). Despite quite different values of α_P, this parameter mainly affects the steepness of the non-linear response curve. The relationship with predator density (micronekton) is estimated to be a decreasing function, with an optimal window at

very low predator densities, around 0.1 g/m^2 in the reference model (see Figure 8, panel Reproduction).

In the model with Lorenzen mortality, the estimated reproduction rate is two orders of magnitude higher than in the reference model. This is a compensatory effect of the much higher early life stages and juvenile mortality imposed by the Lorenzen function, which is inversely related to growth (Figure 8, panel Mortality). As a result, this model produced unrealistically high densities of larvae and small juveniles required to sustain stock levels under current fishing pressure (Figure 8, panel Reproduction and Figure 22). Both models estimate a stock-recruitment relationship characterized by a non-linear functional shape.

6.1.2 Natural mortality rates

Uncertainty remains in the estimation of natural mortality rates at age due to their correlations with reproduction and fisheries parameters, mainly selectivities. In the reference model, the selectivities for the largest sizes were calibrated and fixed, while the slopes of predation and senescence mortality functions were estimated. As a results, age-specific mortality rates were estimated to vary between 0.8 yr^{-1} and 3 yr^{-1} interval, with the lowest mortality occurring at around 5 months of age and increasing to 3.2 yr^{-1} at the age of 4 years. In optimizations using Lorenzen mortality (with fixed parameters), the selectivities were instead estimated. The Lorenzen function implies high mortality rates for early life stages, with values of 6.1 yr^{-1} for larvae and 3.1 yr^{-1} for 3-months old juveniles, progressively decreasing with age to 1.1 yr^{-1} in older fish. With such mortality rates, population abundance declines rapidly with age, with only 5% of recruits surviving to 21 months of age (compared to 26 months in the reference model). However, older individuals have higher chances of survival in the Lorenzen model compared to the reference model. These differences in mortality-at-age functions lead to markedly different estimates of recruit abundance, which is significantly higher in the model with Lorenzen mortality. Nevertheless, estimates of adult and total abundance remain very similar between two models, indicating robustness in their estimation (Figure 22).

6.1.3 Feeding habitats and movement

The estimated directed movement rates are lower than those in the previous reference model. However, because the diffusivity in this model is more than twice smaller, the overall movement pattern remains advective, i.e., characterized by the predominance of directed over random (diffusion) movements. Note, Figure 8 illustrates the density speeds resulting from the combined effects of passive drift (due to ocean currents) and active swimming behaviour of tunas. The decline in movement speed with age reflects the reduced influence of currents on older (and thus larger) individuals. The effect of passive movement on juveniles and adults can be illustrated by a simulation with directed movement set to zero. As shown in Figure 30, which presents the predicted distributions of skipjack tuna under passive movement only, the model fails to reproduce the distribution that explains observed high catches in the western tropical Pacific (see Figures 3 and 20). Consequently, all likelihood components deteriorate markedly when active movement is excluded. Other implications of movement estimation are presented and discussed in section 6.3.3 below.

Regarding thermal preferences that influence the accessibility of prey biomass to skipjack tuna, the reference model estimates a preferred temperature range from approximately 29°C for the youngest individuals to 25°C for the oldest. In contrast, the Lorenzen-ref model yields a narrower range of 27.5–29°C, suggesting a contraction of suitable habitat to the warmest waters. This narrower thermal window introduces a bias in the diffusion rate estimates, artificially facilitating skipjack movement into cooler regions. As a result, the likelihood terms for the EPO fisheries are notably degraded in the Lorenzen-ref model compared to the reference model.

6.1.4 Catchabilities and selectivities

The estimated and fixed values of fisheries parameters are presented in Table 4. Catchabilities were estimated for the fisheries with effort-based catch prediction model (Table 2). During the parameter estimation period, only the longline fishery was allowed to have linearly changing catchability. All pole-and-line fisheries were assumed to have constant catchability between 1991 and 2012. These assumptions seem to be justified given the findings by Nishimoto *et al.* (2024) on technological developments in Japanese fisheries. As a result, residual error for all pole-and-line fisheries during this period shows no temporal bias. In contrast, to achieve a good fit for pole-and-line fisheries during earlier period, the catchabilities for P3, P21, P22, and P15 had to be allowed to increase over time, which indicates that they were continuously development prior to 1991. Moreover, Japanese fisheries had to be split into two fisheries because their catchabilities and rate of increase differed, with the fastest rate estimated during 1982-1989 (see Figure 9), which is consistent with independent modelling study (Nishimoto *et al.*, 2024).

Since the mortality-at-age was fixed in the model with Lorenzen mortality, the selectivities at L_{inf} for major fisheries were estimated. These estimates yielded notably different values across fisheries, except for fishery S5, the FAD-associated purse-seine fishery, which primarily catches young skipjack aged 9-18 months, a range where mortality rates are similar between two mortality functions. However, estimating selectivities did not allow optimizations to improve the fit to length frequency data by fishery. On the contrary, the fit worsened for all purse-seine fisheries under the Lorenzen mortality model, with the most notable deterioration of the LF likelihood for the free school purse-seine fisheries S7.

6.2 Validation

The statistical metrics of model validation with independent catch, length frequency, tag recapture and early-life history data are shown in Figures 10-15.

The fit to the catch data by fishery and for the total catch by region (Figure 10 were evaluated on the MLE dataset including 13 fisheries, and on the entire dataset including 18 fisheries (Table 2). The fit to catch data does not deteriorate when independent data from 1979 to 1994 and from 2013 to 2022 are added to validation. Thus, for the MLE data only, the explained variance, the variance ratio and the normalized mean square error are 0.84, 0.71, 0.41 respectively, and for the 1979-2022 with added 5 fisheries, they yield 0.82, 0.73 and 0.43.

For the length frequency data, all large-scale fisheries pass the NRMSE and standard-

ized bias thresholds (see Figure 11). The only exceptions are two small fisheries, S13 and P14 (see description in Table 2), operating seasonally in the south-west Pacific catching skipjack as by-catch species and providing scarce information on size frequencies.

Model predictions based on the estimated movement and habitat parameters were validated using independent tagging data not included in the likelihood estimation. Comparisons between observed and predicted recapture distributions, along with corresponding one-dimensional profiles and RNMSE metrics, were done by tagging campaign and by region: the tropical western and central Pacific Ocean (Figure 12), the sub-tropical western and central Pacific Ocean (Figure 13), and the eastern Pacific Ocean (Figure 14). The best fit was observed in the tropical WCPO during the large-scale tagging campaigns of 2007–2015 (note, the MLE tag groups, as shown in Figure **??**, are not included in these plots). For earlier tagging periods (1979–1993 and 1994-2005), the fit is less accurate, though the metrics are still comparable to that obtained for the MLE groups of tags, with NRMSE(lon)=0.73 and NRMSE(lat)=0.27 in the tropical WCPO.

In modelling the feeding migration of skipjack toward the Kuroshio Extension, the zonal movements were reasonably well captured — even with a limited number of tags — while meridional movements remained poorly reproduced. An exception is the 1988–1999 tagging period, during which skipjack were released and recaptured while migrating; in this case, intermediate displacements between the tropical zone and the Kuroshio Extension were reasonably well reproduced as shown by the latitudinal profile in Figure 13. However, in general, the model does not predict skipjack reaching the northernmost extent of their observed feeding grounds.

In the EPO, where the model did not have tagging data to learn about the movement and habitats, it nevertheless captures the movement patterns observed during the 2006 and 2019–2022 tagging campaigns. However, a zonal bias is evident, with the model displacing some tags farther east than observed or farther west for the 1979-1981 tags, which were released closer to the Central America's coasts.

Validation of skipjack larval distributions at early developmental stages is presented in Figures 15 and 16. In general, incorporating early-life history data into the model and estimating model parameters using all data likelihoods improved observability of adult stock distribution, hence contributed to better estimation of movement rates. This was revealed by the improved statistical scores for tagging data and better convergence to valid MLEs compared to the model without the early-life data likelihood. An independent evaluation of the model's predictive skill for this type of data was conducted using: 1) the NRMSE metric for larval distributions at four environmental variables, and 2) linear correlations between normalized seasonal densities, evaluated for the years 1960-1981, closely matching the observational dataset timeframe (1956-1981). All NRMSE values indicated very good agreement between observed and predicted frequencies. Seasonal patterns were well reproduced across most regions, except in the tropical area north of the equator and west of 180°E, where coefficients of correlation are relatively low (0.23 and 0.45). In this region, the model does not predict a seasonal decline in larval densities during July-September months. Note that from the preliminary estimation of early-life parameters using the spawning habitat model, these correlations were much lower (0.07 and -0.11), and overall performance across regions was poorer compared to the outputs of the dynamic model. This suggests that the density of adult skipjack population is a key variable that determines the seasonality of larval density distributions.

6.3 Predicted spatiotemporal dynamics

Skipjack population structure predicted with estimated model parameters (Figure 17) and the total stock biomass (Figure 18) are similar to the previous reference model (Senina *et al.*, 2019). However, compared to the previous reference model, estimated using fisheries and tagging data, the new solution reveals more variable temporal dynamics, reflecting the influence of interannual and decadal variability in the tuna environment (see Figure 1 and 18). The model predicts a general decline in population biomass — both exploited and unfished (virgin) stock — during the first 35 years of simulation (Figure 18). This period includes the well-documented 1977 climate regime shift, which is reflected by the peak in total WCPO biomass in the following year. Subsequently, during the positive phase of the Interdecadal Pacific Oscillation (IPO), characterized by warmer sea surface temperatures (SSTs) in the central and eastern tropical Pacific, and resembling a prolonged El Niño-like conditions, skipjack biomass continued to decline until the end of 1994. From 1995 onward, the stock experienced several strong ENSO events (1997–2001, 2009–2012, 2015–2016, 2020–2022) and a shift toward longer-lasting La Niña conditions associated with a negative IPO phase. These cooler, more productive conditions supported higher recruitment and helped sustain skipjack biomass despite substantial fishing pressure. Notably, the F_0 simulation (no fishing) shows that under these conditions, the biomass would have increased further in the absence of exploitation.

Spatial distributions of skipjack biomass density show highest concentrations of skipjack in the warm waters of the western equatorial Pacific, explaining the high catches there (see Figures 19 and 20). The main western stock, although well connected, seems to be split in two sub-stocks by the equatorial countercurrent, with the southern sub-stock having higher biomass densities locally. The EPO stock is much more spread across the region. Here the highest densities of skipjack are predicted along the coasts of Central and South Americas, mainly in the zones of coastal upwelling and local productivity hotspots. e.g., Galapagos and NECC convergence zone. Seasonally, skipjack is predicted to migrate to the productive waters of Kuroshio Extension and Peruvian upwelling although these movements are still biased because of misrepresentation of ocean dynamics with 1° resolution (see Figure 19). It should be noted also that the spatial distributions are highly dynamic and differ from one year to another driven by environmental inter-annual variability. Marked seasonality is estimated for skipjack recruits, in particular in the EPO (Figure 20).

Due to differences in reproduction, habitat and movement parameters, the model with Lorenzen mortality estimates more western and tropical skipjack stock (Figure 21), with reduced sub-tropical and EPO biomass. However the total stock over the Pacific Ocean domain remains nearly the same (Figure 22).

In terms of movement, the connectivity between assessment regions (see regional structure in Figure 24) was evaluated for both models, but since the movement probabilities are qualitatively similar, we focus here on the results from the reference model only (Figure 23). It was found that in the WCPO, the biomass moves actively through the equatorial regions 6, 7 and 8, with adult biomass exchange occurring primarily with assessment region 4. The regions north of 10°N are interconnected, with net movement following a clockwise pattern. The Indo-Pacific region (assessment region 5) acts a a biomass sink for adult skipjack biomass, contributing to other regions only through larval drift from its

north-east quadrant (130°E-140°E, 0°-10°N) to adjacent regions. In contrast, it receives juvenile and adult biomass from assessment region 3.

6.3.1 Stock estimation and comparisons with MULTIFAN-CL

The total skipjack biomass in the WCPFC statistical area is estimated to be 7.1 million metric tons (Mt), based on the five-year average from 2018 to 2022 (Figure 1). The corresponding Pacific-wide biomass, including the Indo-Pacific region (100°E-70°W, 20°S-45°N) is 9 Mt, hence the EPO region contributing approximately 1.9 Mt.

SEAPODYM estimates bigger stock of skipjack in the WCPO than MULTIFAN-CL (Castillo Jordán *et al.*, 2022). The estimates from two models are consistent in terms of overall trends and recruitment levels for the period 1994–2019. Also, despite some regional differences, total biomass estimates align closely when considering only the eastern regions (2, 4, 7 and 8). Therefore, the overestimation of biomass in SEAPODYM, compared to the stock assessment model, originates primarily from regions characterized by warmest ocean or warm current systems (Kuroshio current), which the MLE approach identifies as the most suitable environment for skipjack (Figure 25).

However, the models diverge for earlier years from 1972 to 1993: MULTIFAN-CL predicts an increasing trend in both recruitment and total biomass, whereas SEAPODYM indicates a decline in both estimates during that period (see Figures 24–25). The declining trend in SEAPODYM is primarily driven by the positive phase of the Interdecadal Pacific Oscillation (IPO), which was characterized by reduced ocean productivity in the western Pacific Ocean. In contrast, the trend captured by MULTIFAN-CL is influenced by Japanese pole-and-line CPUE indices (Hamer *et al.*, 2024). Notably, a recent study (Nishimoto *et al.*, 2024) suggests that the catchability of the pole-and-line fishery may have increased by as much as four-fold between the early 1970s and the 1990s, which could have biased historical abundance trends inferred from those fisheries' CPUEs.

6.3.2 Fisheries impact

The fishing impact is evaluated for 2020 due to incomplete geo-referenced catches in 2021-2022 (see Figure 2). The impact by fishing is assessed as $FI = 1 - B_F(t)/B_{F=0}(t)$ or as a depletion ratio across ages $B_F(a)/B_{F=0}(a)$ (Figure 26). SEAPODYM estimates the stock reduction from virgin biomass by 26.5% for the WCPFC stock, 15.6% for the EPO region, resulting in 24% biomass reduction over the entire Pacific Ocean. Locally, 50% biomass reduction are estimated in the WCPO and 40% biomass reduction in the EPO (Figure 27). Note that these figures are likely underestimated due to the exclusion of catches from Japanese fisheries north of 35°N and the lack of catches not included in the geo-referenced datasets.

6.3.3 Impacts of environmental variability on movement and recruitment

Environmental variability influences both recruitment and movement of skipjack tuna. As previously reported by Lehodey *et al.* (1997), El Niño events cause an eastward expansion of warm surface waters in the equatorial Pacific, leading to the shift of skipjack tuna distribution eastward in response to changing habitat conditions. This pattern is clearly reflected in the Hovmöller diagrams of total skipjack biomass between 140°E and 120°W

(Figure 28) predicted by the current reference model. To quantify these shifts, barycentres of total equatorial biomass, as well as those of the northern and southern sub-stocks, were computed. They show that the biomass distributions can shift by more than 20° in one year. Moreover, Figures 28 and 29 illustrate that skipjack in the Northern Hemisphere tend to move farther eastward into the central Pacific compared to those in the Southern Hemisphere. Additionally, the southern stock appears constrained by the 29°C isotherm, a limitation not observed for the northern sub-stock.

To better understand the underlying mechanisms, observed zonal displacements were further investigated to determine the role of ocean currents in driving the skipjack biomass. As proposed by Barrier *et al.* (2023), ocean currents are a primary driver of ENSO-induced zonal movements of skipjack tuna. To isolate their effect, additional simulations were conducted in which all model parameters were fixed at their maximum likelihood estimates, except for movement, which was limited to passive advection. As shown in Figure 30, the resulting skipjack distributions differ notably from the reference model: the southern sub-stock becomes more dispersed, while the northern sub-stock shifts farther north and stretches longitudinally across the Pacific. While these additional simulations confirmed that ocean currents contribute to eastward displacements, the full pattern of skipjack redistribution emerges from the interplay of physical processes (currents) and fish behaviour (active swimming and habitat selection).

The reference model reveals a persistent eastward shift in total skipjack biomass within the WCPO from 1960 to 2022, likely reflecting the influence of climate change (Figure 29). One of the indications that the model captures a long-term climate signal across the historical period, is that this shift occurs more rapidly in the northern sub-stock, which is consistent with observed faster rates of warming in the Northern Hemisphere relative to the Southern Hemisphere (see e.g., Stouffer *et al.*, 2004). This result will be further explored using simulations forced by an ensemble of Earth System Models. Importantly, despite observed zonal shifts, the model does not predict a significant meridional expansion of the skipjack biomass.

Bibliography

Barrier, N., Lengaigne, M., Rault, J., Person, R., Ethe, C., Aumont, O., and O. Maury. 2023. Mechanisms underlying the epipelagic ecosystem response to ENSO in the tropical Pacific. Progress in Oceanography, 208, 103002. https://doi.org/10.1016/j.pocean.2023.103002

Bell, J., Senina, I., Adams, T., ... Tsamenyi, M., Williams, P. 2021. Pathways to sustaining tuna-dependent Pacific Island economies during climate change. Nature Sustainability, 2021, 4(10), pp. 900–910.

Bonnin, L. and I. Senina. 2024. SEAPODYM: Integration of new data to inform modelling of tuna's early life stages dynamics. In The 20st Regular Session of the Scientific Committee of the Western Central Pacific Fisheries Commission, 14–21 August 2024, Manila, Philippines. Volume WCPFC-SC20-2024/EB-IP-33.

Buenafe, K.C.V., Everett, J.D., Dunn, D.C. et al. 2022. A global, historical database of tuna, billfish, and saury larval distributions. Sci Data 9, 423. https://doi.org/10.1038/s41597-022-01528-7.

Buenafe, K.C.V., et al. (in press). Near-global spawning strategies of large pelagic fish. Nature Communications. Pre-print available at https://www.researchsquare.com/article/rs-4532139/v1.

Brill, R. 1994. A review of temperature and oxygen tolerance studies of tunas pertinent to fisheries oceanography, movement models and stock assessments. *Fisheries Oceanography* 3:3, 204-216.

Castillo Jordán, C., Teears, T., Hampton, J., Davies, N., Scutt Phillips, J., McKechnie, S., Peatman, T., MacDonald, J., Day, J., Magnusson, A., Scott, R., Scott, F., Pilling, G., and P. Hamer. 2022. Stock assessment of skipjack tuna in the western and central Pacific Ocean. In The 18th Regular Session of the Scientific Committee of the Western Central Pacific Fisheries Commission, 10–18 August 2022, Online, Volume SC18-SA-WP-01 - Rev.05.

1989. Tuna Larvae Abundance: Comparative Estimates from Concurrent Japanese and Australian Sampling Programs. Fishery Bulletin, U.S. 87:976–981. 1989.

Forestier, R., Bonnin, L., Senina, I., Vidal, T., Ghergariu, M., and S. Nicol. A comprehensive method to integrate unbiased fisheries data in spatially-explicit population dynamics models. In The 21st Regular Session of the Scientific Committee of the Western Central Pacific Fisheries Commission, 13 – 21 August 2024, Nuku'alofa, Tonga. Volume WCPFC-SC21-2025/SA-IP-21.

Fujioka, K., Aoki, Y., Tsuda, Y., Okamoto, K., Tsuchida, H., Sasaki, A., and H. Kiyofuji. 2024. Influence of temperature on hatching success of skipjack tuna (Katsuwonus pelamis): Implications for spawning availability of warm habitats. *Journal of Fish Biology* DOI: 10.1111/jfb.15767

Graham, J. B., Dickson, K. A. 2004. Tuna comparative physiology. *The Journal of Experimental Biology* 207: 4015-4024. doi:10.1242/jeb.01267

Nishimoto M., Aoki Y., Matsubara N., Hamer P. and Tsuda Y. 2024. Investigating long-term recruitment trends of skipjack tuna in the Western and Central Pacific Ocean and Effort Creep in the Japanese Pole and Line Skipjack Fishery (WCPFC Project: 115). In The 20st Regular Session of the Scientific Committee of the Western Central Pacific Fisheries Commission, 14 – 21 August 2024, Manila, Philippines. Volume WCPFC-SC20-2024/SA-WP-06.

Hampton, J., and Fournier, D.A. 2001. A spatially disaggregated, length-based, age- structured population model of yellowfin tuna (Thunnus albacares) in the western and central Pacific Ocean. Mar. Freshw. Res. 52: 937–963. https://doi.org/10.1071/MF01049.

The IATTC Program for In-Port Sampling of Tuna Catches. SAC-01-11 Document. Inter-American Tropical Tuna Commission, Scientific Advisory Committee 1st Meeting, 31 August - 3 September 2010, La Jolla, California, USA.

Description of larvae and distribution of four species of tuna in central Pacific waters. US Dept. of Interior, Fish and Wildlife Service, Fishery Bull. 58: 31-72.

McKechnie, S., Hampton, J., Pilling, G.M., and Davies, N. 2016. Stock assessment of skipjack tuna in the western and central Pacific Ocean. In The 12th Regular Session of the Scientific Committee of the Western Central Pacific Fisheries Commission, 3–11 August 2016, Bali, Indonesia. Volume WCPFC-SC12-2016/SA-WP-04.

Lehodey, P., Bertignac, M., Hampton, J., Lewis, A., Picaut, J. 1997. El Niño Southern Oscillation and tuna in the western Pacific. *Letters to Nature.* 389, 715-718.

Nicol,S., Dessert, M., Gorgues, T., Aumont, O., Menkes, C., P. Lehodey. 2014. Progress report on climate simulations. WCPFC-SC10-2014/EB-IP-02.

Nishikawa, Y., Honma, M., Ueyanagi, S., and Kikawa, S. 1985. Average Distribution of Larvae of Oceanic Species of Scombroid Fishes, 1956–1981. (Far Seas Fisheries Research Laboratory, 1985).

Nishimoto M., Aoki Y., Matsubara N., Hamer P. and Tsuda Y. 2024. Estimating fish stock biomass using a Bayesian state-space model: accounting for catchability change due to technological progress. Front. Mar. Sci. 11:1458257. doi: 10.3389/fmars.2024.1458257

Nooteboom, P., Scutt Phillips, J., Senina, I., van Sebille, E., and Nicol, S. 2023. Individual-based model simulations indicate a non-linear catch equation of drifting Fish Aggregating Device-associated tuna. ICES Journal of Marine Science, 2023, 80, 1746–1757. https://doi.org/10.1093/icesjms/fsad105.

Otter Research Ltd. 1994. Autodif: a C++ array extension with automatic differentiation for use in nonlinear modeling and statistics. Otter Research Ltd: Nanaimo, Canada.

Pacific Community (SPC). 2022. Tuna Fisheries Yearbook. Western and Central Pacific Fisheries Commission, Pohnpei, Federated States of Micronesia.

Global multi-year biogeochemical hindcast (1998–2023) using SEAPODYM-LMTL", Copernicus Marine Environmental Service, 30 June 2024. Quality Information Document — CMEMS-GLO-QUID-001-033.

Scholey, V., Bromhead, D., Margulies, D., Nicol, S., Wexler, J., Santiago, M., Williamson, J.E., Hoyle, S., Schlegel, P., Havenhand, J., Ilyina, T., and P. Lehodey. 2012. Novel Research Into the Impacts of Ocean Acidification Upon Tropical Tuna. PFRP Newsletter, V. 16/1.

Scutt Phillips, J., Lehodey, J., Hampton, J., Hamer, P., Senina, I., and S. Nicol. 2022. Quantifying Rates of Mixing in Tagged, WCPO Skipjack Tuna. In The 18th Regular Session of the Scientific Committee of the Western Central Pacific Fisheries Commission, 10–18 August 2022, Online, Volume SC18-SA-WP-04.

SEAPODYM: spatial ecosystem and population dynamics model for migratory age-structured stocks [version 4.0]. Reference Manual, Pacific Community, 186pp. https://purl.org/spc/digilib/doc/vxsz3

Senina I.N., Sibert, J.R., Lehodey P. 2008. Parameter estimation for basin-scale ecosystem-linked population models of large pelagic predators: Application to skipjack tuna. *Progress in Oceanography* 78, 319-335.

Senina, I., Lehodey P., Sibert J., Hampton J., 2020. Improving predictions of a spatially explicit fish population dynamics model using tagging data. Can. J. Fish. Aquat. Sci., 18 pp, dx.doi.org/10.1139/cjfas-2018-0470.

Senina, I., Lehodey P., Hampton J., Sibert J. 2020. Quantitative modelling of the spatial dynamics of South Pacific and Atlantic albacore tuna populations. Deep Sea Research II, doi.org/10.1016/j.dsr2.2019.104667.

Senina, I., Briand, G., Lehodey, P., Nicol, S., Hampton, J., Williams, P. 2021. Reference model of bigeye tuna using SEAPODYM with catch, length and conventional tagging data. Western and Central Pacific Fisheries Commission Scientific Committee, Information Paper. WCPFC-SC17-2021/EB-IP-08.

Sibert, J.R., Hampton, J., Fournier, D.A., Bills, P.J. 1999. An advection-diffusion-reaction model for the estimation of fish movement parameters from tagging data, with application to skipjack tuna (*Katsuwonus pelamis*). *Can. J. Fish. Aquat. Sci.* 56, 925-938.

Stouffer, R. J., Broccoli, A. J., Delworth, T. L., Dixon, K. W., Spelman, M. J., and Stern, W. F. 2004. North–South asymmetry in climate response to increased atmospheric CO_2 concentrations. Nature, 429(6994), 263–267. https://doi.org/10.1038/nature02581.

Estimated of larval tuna abundance in the Central Pacific, Fish and Wildlife Service, Fishery Bull. 167, Volume 60: 31-72.

List of Tables

7 Tables

Table 1: Forcing variables used in current SEAPODYM model. Note that table shows original resolutions, all variables were then interpolated to spatial and temporal resolutions 2° x 30 days and 1° x 30 days.

Variable	Description	Resolution	Time period
	NEMO		
T, u, v, SST, MLD	Physical variables simulated by NEMO ocean general circulation model forced by atmospheric JRA55 reanalysis	ORCA1, daily	1958 - 2022
	PISCES		
P, Z, O_2	Primary production, euphotic depth and dissolved oxygen variables simulated by the PISCES model coupled with NEMO OGCM	ORCA1, daily	1958 - 2022
	LMTL		
F	Six micronekton groups simulated by the LMTL model with the NEMO-PISCES forcing and parametrization described in QUID (2024)	1°, 30 days,	1958 - 2022

Table 2: Skipjack fisheries structure. NWCPO stands for North-West and Central Pacific, TPO - for Tropical Pacific Ocean, SWPO - for South-West Pacific Ocean. C-model column provides information on the catch observation (prediction) model, where CR refers to catch removal method and effort refers to more classical Gordon-Schaefer method based on fishing effort.

ID	Gear	Region	Flag-Fleet	School	$\Delta x \cdot \Delta y$	Time period	C-model
P1	PL	NWCPO	JP-OS	None	1x1	1972-2022	Effort
P2	PL	NWCPO	JP-DW	None	1x1	1972-2003	Effort
P21	PL	WCPO	JP-DW	None	1x1	1972-1981	Effort
P22	PL	WCPO	JP-DW	None	1x1	1982-1989	Effort
P23	PL	WCPO	JP-DW	None	1x1	1990-2022	Effort
P3	PL	TPO	All	None	1x1	1970-2022	Effort
S4	PS	NWCPO	JP	All	1x1	1970-2023	CR
S5	PS	WCPO	All	Log, dFAD, aFAD	1x1	1968-2023	CR
S6	PS	WCPO	PH,ID	All	1x1	1951-2023	CR
S7	PS	WCPO	All	Free schools and animals	1x1	1967-2023	CR
L8	LL	PO	All	None	5x5	1950-2023	Effort
O9	Mix	WCPO	All	None	1x1	1950-2022	CR
S10	PS	EPO	All	Log, dFAD, aFAD	1x1	1959-2023	CR
S11	PS	EPO	All	Dolphins	1x1	1959-2020	CR
S12	PS	EPO	All	Free schools	1x1	1958-2023	CR
S13	PS	SWPO	All	All	1x1	1975-2021	CR
P14	PL	SWPO	AU, NZ, JP-DW	None	1x1	1974-2022	Effort
P15	PL	EPO	KR, MX, US	None	1x1	1978-2005	Effort

Table 3: SEAPODYM parameters. Parameters marked by asterisks were fixed in optimization experiment. Parameter with [or] were estimated (and subsequently fixed if asterisk is added) at their lower or upper boundary correspondingly. The dash indicates that the parameter is not effective and could not be estimated.

θ	**Description**	**REF**	**Lorenzen**
	Spawning habitat and reproduction		
σ_0	standard deviation in thermal Gaussian function of spawning habitat, $^\circ C$	10]*	10]*
$T_0^\star$	mean in thermal Gaussian function of spawning habitat, $^\circ C$	35.96	35.43
α_P	prey encounter rate in Holling (type III) function, day^{-1}	7.19	1.71
α_F	mean of log-normal predator-dependent function, g/m^2	2.5]*	2.5]*
β_F	shape parameter of log-normal predator-dependent function	2.17	2.8
R	reproduction rate in Beverton-Holt function, mo^{-1}	1.29	236.26
b	slope parameter in Beverton-Holt function, nb/km^2	0.41	0.49
	Natural mortality		
$\bar{m}_p$	predation mortality rate age age 0, mo^{-1}	0.35*	0.3*
β_p	slope coefficient in predation mortality	0.75]	0.29*
$\bar{m}_s$	senescence mortality rate at age 0, mo^{-1}	0.02]*	0.211*
β_s	slope coefficient in senescence mortality	0.67	-0.22*
ϵ_0	variability of larval mortality rate with spawning habitat index $M_H \in (M, M(1+\epsilon))$	14.36	12.37
ϵ	variability of juvenile and adult mortality rate with feeding habitat index $M_H \in (M, M(1+\epsilon))$	[0*	[0*
	Feeding habitats		
T_0	optimal temperature (if Gaussian function), or temperature range for the first young cohort, $^\circ C$	30.86	30.86
T_K	optimal temperature (if Gaussian function), or temperature range for the oldest adult cohort, $^\circ C$	24.65	27.5
γ	slope coefficient in the function of oxygen)	1e-04]	1e-04]
$\hat{O}$	threshold value of dissolved oxygen, ml/l	4.13	4.0
eF_1	contribution of epipelagic forage to the habitat	1.0	1.12
eF_1	contribution of mesopelagic forage to the habitat	3.5	3.29
eF_1	contribution of migrant mesopelagic forage to the habitat	[0*	[0*
eF_1	contribution of bathypelagic forage to the habitat	[0*	[0*
eF_1	contribution of migrant bathypelagic forage to the habitat	[0*	[0*
eF_1	contribution of highly migrant bathypelagic forage to the habitat	4.16	3.7
	Movement		
V_m	maximal sustainable speed of tuna in body length, BL/sec	0.407	0.35
a_V	slope coefficient in allometric function for maximal speed	[0.3*	[0.3*
σ	multiplier for the maximal diffusion rate	0.4342	0.52
c	coefficient of diffusion variability with habitat index	[0*	0.1

Table 4: Fisheries parameters. Catchabilities are given for validity period of corresponding fishery (Table 2). Selectivities of all fisheries except L8 are asymmetric Gaussian functions, and Selectivity at L_{inf} is the value at maximal length. Parameters marked by asterisks, [or] were fixed or estimated at their lower or upper boundary respectively.

θ	**Description**	**REF**	**Lorenzen**
	Fishery P1		
q_1	Catchability	0.0067	0.0059
s_1	Standard deviation of Gaussian selectivity (cm)	8.5*	8.5*
$\hat{l}_1$	Size at maximal selectivity (cm)	47.71	47.63
$s_{inf,1}$	Selectivity at L_{inf}	0.4*	0.56
	Fishery P2		
q_2	Catchability	0.0087	0.004
s_2	Standard deviation of Gaussian selectivity (cm)	5.46*	5.46*
$\hat{l}_2$	Size at maximal selectivity (cm)	45*	45*
$s_{inf,2}$	Selectivity at L_{inf}	0.1*	1]
	Fishery P21		
q_3	Catchability	0.0013 - 0.0028	0.0013 - 0.0027
s_3	Standard deviation of Gaussian selectivity (cm)	15*	15*
$\hat{l}_3$	Size at maximal selectivity (cm)	57*	57*
$s_{inf,3}$	Selectivity at L_{inf}	0.3*	
	Fishery P22		
q_4	Catchability	0.0034 - 0.0065	0.0051 - 0.0095
s_4	Standard deviation of Gaussian selectivity (cm)	16*	16*
$\hat{l}_4$	Size at maximal selectivity (cm)	55*	55*
$s_{inf,4}$	Selectivity at L_{inf}	0.4*	0.4*
	Fishery P23		
q_5	Catchability	0.0076	0.0109
s_5	Standard deviation of Gaussian selectivity (cm)	15*	15*
$\hat{l}_5$	Size at maximal selectivity (cm)	59.55	60.8
$s_{inf,5}$	Selectivity at L_{inf}	0.7*	0.18
	Fishery P3		
q_6	Catchability	5.2e-04 - 6.7e-04	0.0024
s_6	Standard deviation of Gaussian selectivity (cm)	10*	10*
$\hat{l}_6$	Size at maximal selectivity (cm)	52.72	52.83
$s_{inf,6}$	Selectivity at L_{inf}	0.1*	0.14
	Fishery S4		
s_7	Standard deviation of Gaussian selectivity (cm)	5.5*	8.8
$\hat{l}_7$	Size at maximal selectivity (cm)	49.5*	52.5*
$s_{inf,7}$	Selectivity at L_{inf}	0.25*	0.58*
	Fishery S5		
s_8	Standard deviation of Gaussian selectivity (cm)	12.5*	12.75
$\hat{l}_8$	Size at maximal selectivity (cm)	52.79	53.82
$s_{inf,8}$	Selectivity at L_{inf}	0.3*	0.35
	Fishery S6		
s_9	Standard deviation of Gaussian selectivity (cm)	15*	15*
$\hat{l}_9$	Size at maximal selectivity (cm)	49*	49*
$s_{inf,9}$	Selectivity at L_{inf}	0*	0*

	Fishery S7		
s_{10}	Standard deviation of Gaussian selectivity (cm)	12.5*	21.87
$\hat{l}_{10}$	Size at maximal selectivity (cm)	61.47	70.48
$s_{inf,10}$	Selectivity at L_{inf}	0.4*	[0
	Fishery L8		
q_{11}	Catchability	1e-04 - 3e-04	4e-5 - 1e-4
s_{11}	Slope of selectivity function	0.18*	0.19*
$\hat{l}_{11}$	Size at 50% selectivity (cm)	76*	64*
	Fishery O9		
s_{12}	Standard deviation of Gaussian selectivity (cm)	11*	11*
$\hat{l}_{12}$	Size at maximal selectivity (cm)	40*	40*
$s_{inf,12}$	Selectivity at L_{inf}	0.2*	0.2*
	Fishery S10		
s_{13}	Standard deviation of Gaussian selectivity (cm)	7.5*	7.5*
$\hat{l}_{13}$	Size at maximal selectivity (cm)	43.66	44.71
$s_{inf,13}$	Selectivity at L_{inf}	0.9*	0.6*
	Fishery S11		
s_{14}	Standard deviation of Gaussian selectivity (cm)	15*	14.63
$\hat{l}_{14}$	Size at maximal selectivity (cm)	59.5	60.1
$s_{inf,14}$	Selectivity at L_{inf}	0.8*	[0.1
	Fishery S12		
s_{15}	Standard deviation of Gaussian selectivity (cm)	10*	17.33
$\hat{l}_{15}$	Size at maximal selectivity (cm)	53.22	63.48
$s_{inf,15}$	Selectivity at L_{inf}	0.85*	0.18
	Fishery S13		
s_{16}	Standard deviation of Gaussian selectivity (cm)	10*	10*
$\hat{l}_{16}$	Size at maximal selectivity (cm)	49.85*	49.85*
$s_{inf,16}$	Selectivity at L_{inf}	0.2*	0.2*
	Fishery P14		
q_{17}	Catchability	0.016*	0.016*
s_{17}	Standard deviation of Gaussian selectivity (cm)	6.5*	6.5*
$\hat{l}_{17}$	Size at maximal selectivity (cm)	48.5*	48.5*
$s_{inf,17}$	Selectivity at L_{inf}	0.3*	
	Fishery P15		
q_{18}	Catchability	0.012 - 0.016	0.02
s_{18}	Standard deviation of Gaussian selectivity (cm)	15*	15*
$\hat{l}_{18}$	Size at maximal selectivity (cm)	60*	60*
$s_{inf,18}$	Selectivity at L_{inf}	0.5*	0.5*

List of Figures

8 Figures

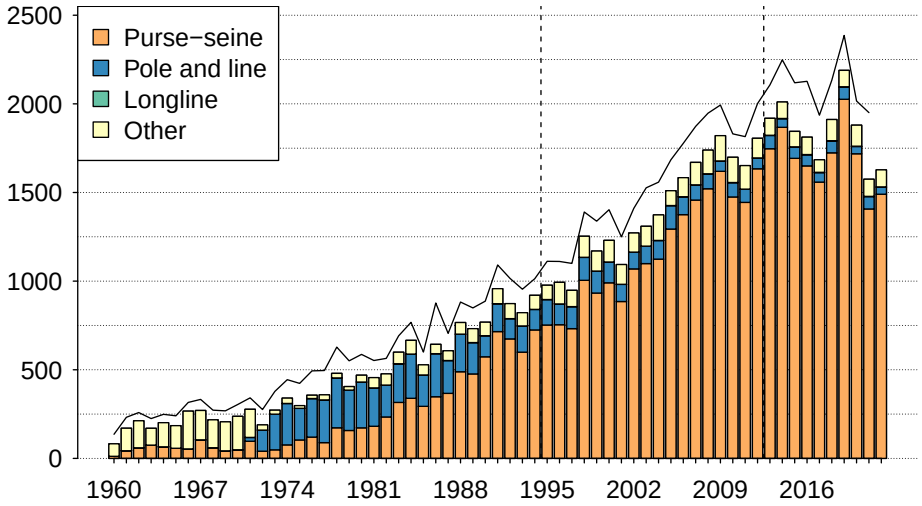

Figure 2: Total annual skipjack catch aggregated from geo-referenced catch (Pacific-wide) used in SEAPODYM analyses. Solid line corresponds to total landings of skipjack (SPC Yearbook, 2019). Dashed vertical lines indicate the data being used in MLE.

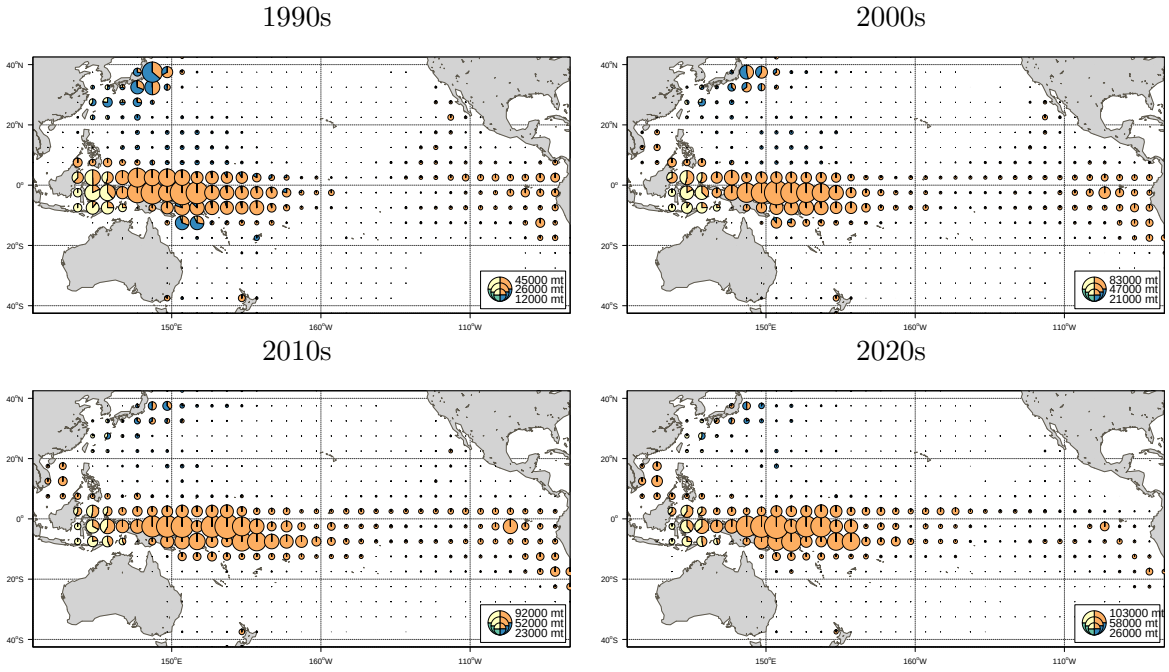

Figure 3: Spatial distributions of catches by decade and by gear: longline (orange), purse-seine (blue), pole-and-line (green), and others (yellow).

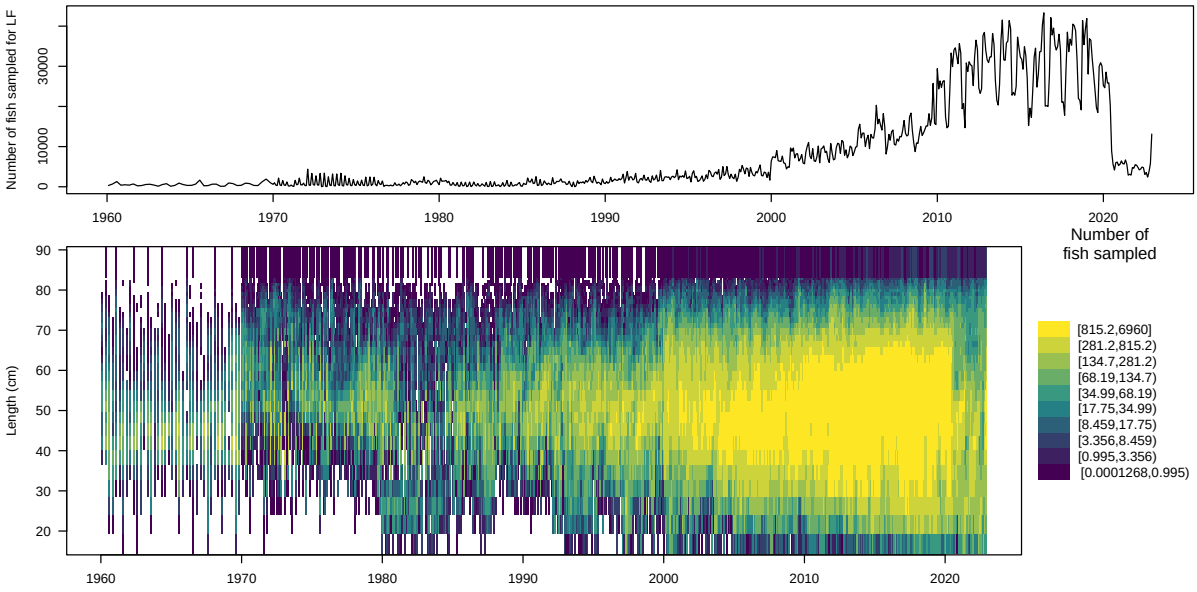

Figure 4: Skipjack length frequency data coverage. The time series on the top panel shows the total number of fish being sampled over the Pacific Ocean and the color map on the bottom panel shows the time evolution of the total number of fish sampled by length bin.

a) WCPO

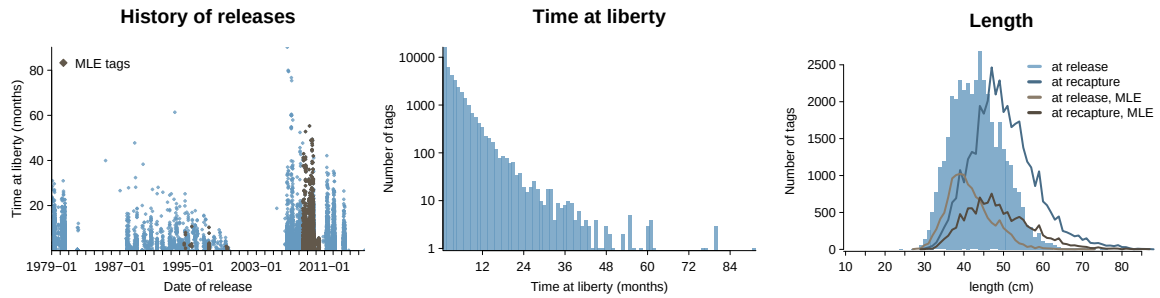

b) EPO

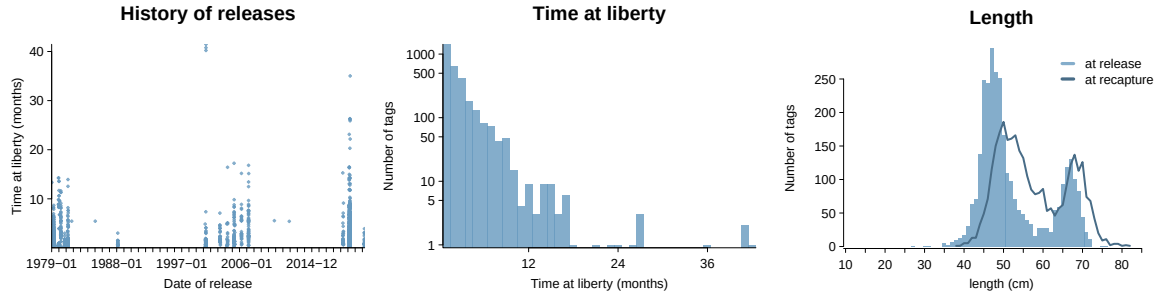

Figure 5: WCPO and EPO tagging data: history of tag releases with the time at liberty shown to each record; time at liberty histogram; and length of tagged fish at release and recapture. Note, the diamonds and additional length distributions of tags at release and recapture shown with darker color indicate the data being used in MLE.

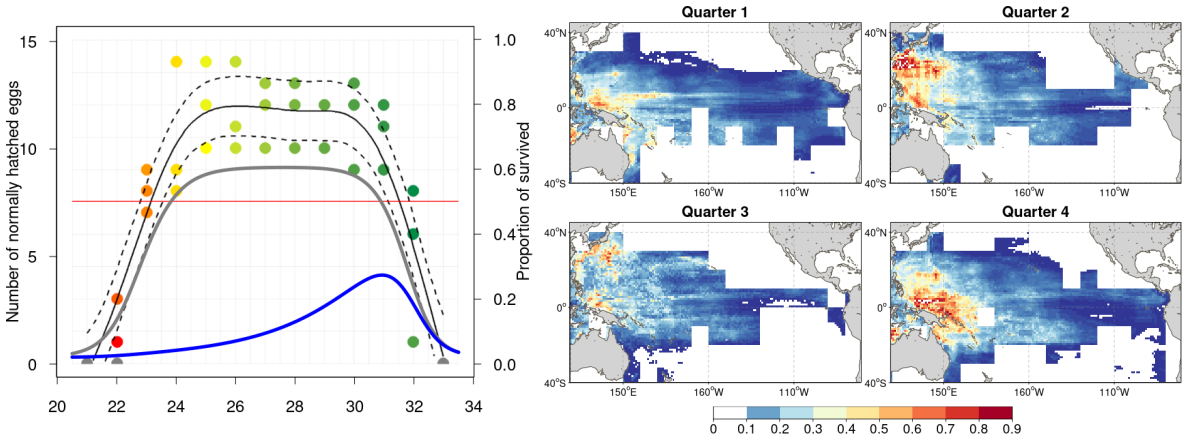

Figure 6: Early-life history data: (left) filled circles and thin black lines show the number of normally hatched skipjack eggs as a function of temperature from Fujioka et al. (2024) study, the grey and blue lines corresponds to the proportion (right y-axis) of eggs and larvae surviving in the reference model at one week of age correspondingly; (right) probability of larvae occurrence predicted by boosted regression tree model from digitized larval sampling data (Buenafe et al., 2022).

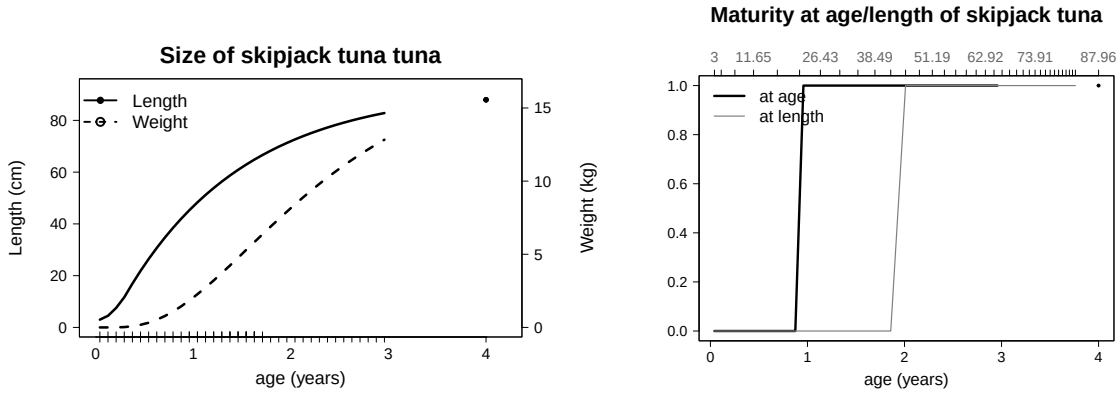

Figure 7: Static model parameters: (left) mean length and weight interpolated from McKechney et al. (2016) at the mid-point of each monthly age class indicated with the outer tick marks of the x-axis. The inner ticks of the x-axis show the ages when the habitat indices are evaluated; (right) maturity at age or length (upper x axis).

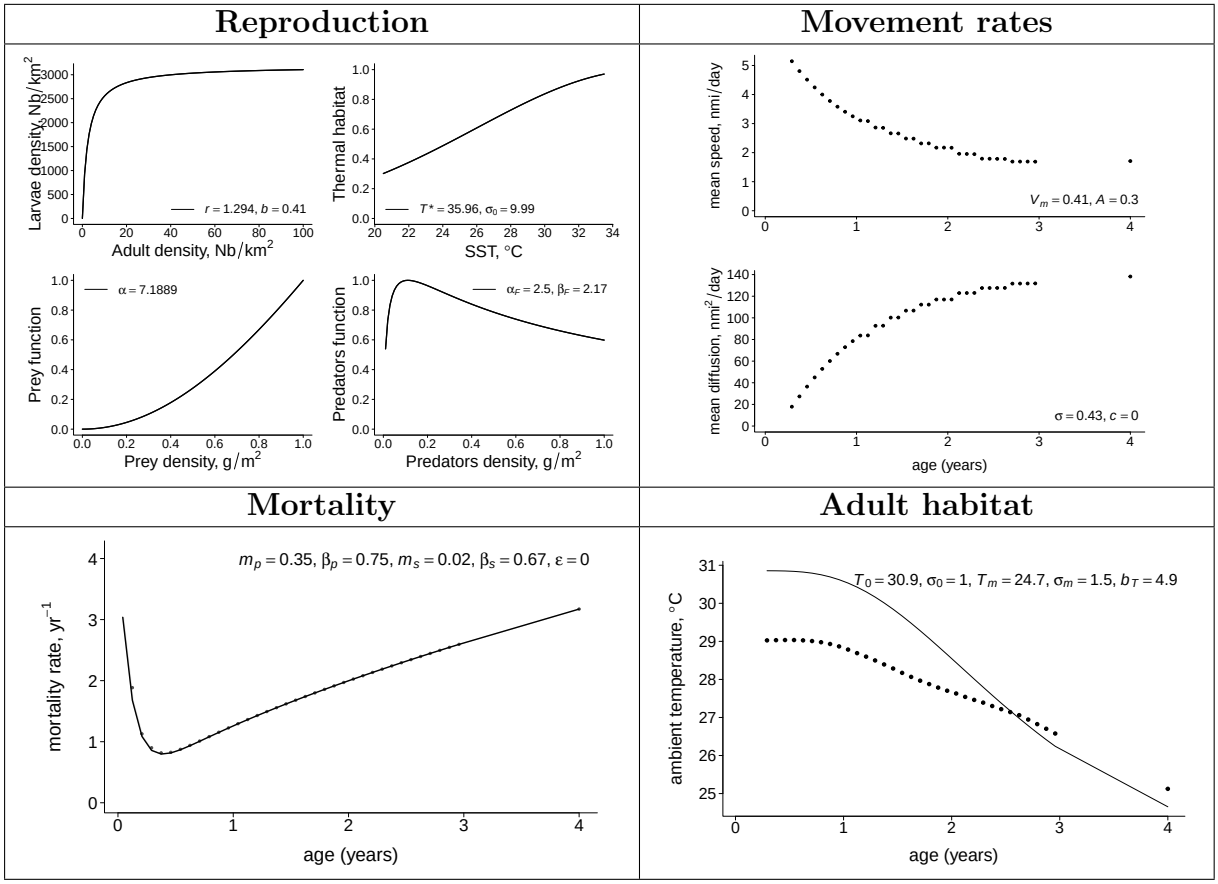

Figure 8: Estimated functional relationships in main dynamical processes (reproduction, natural mortality and movement) of reference MLE model constrained by fisheries data only. Habitat temperature and movement rates are computed as weighted spatio-temporal average with weights being the population density at age.

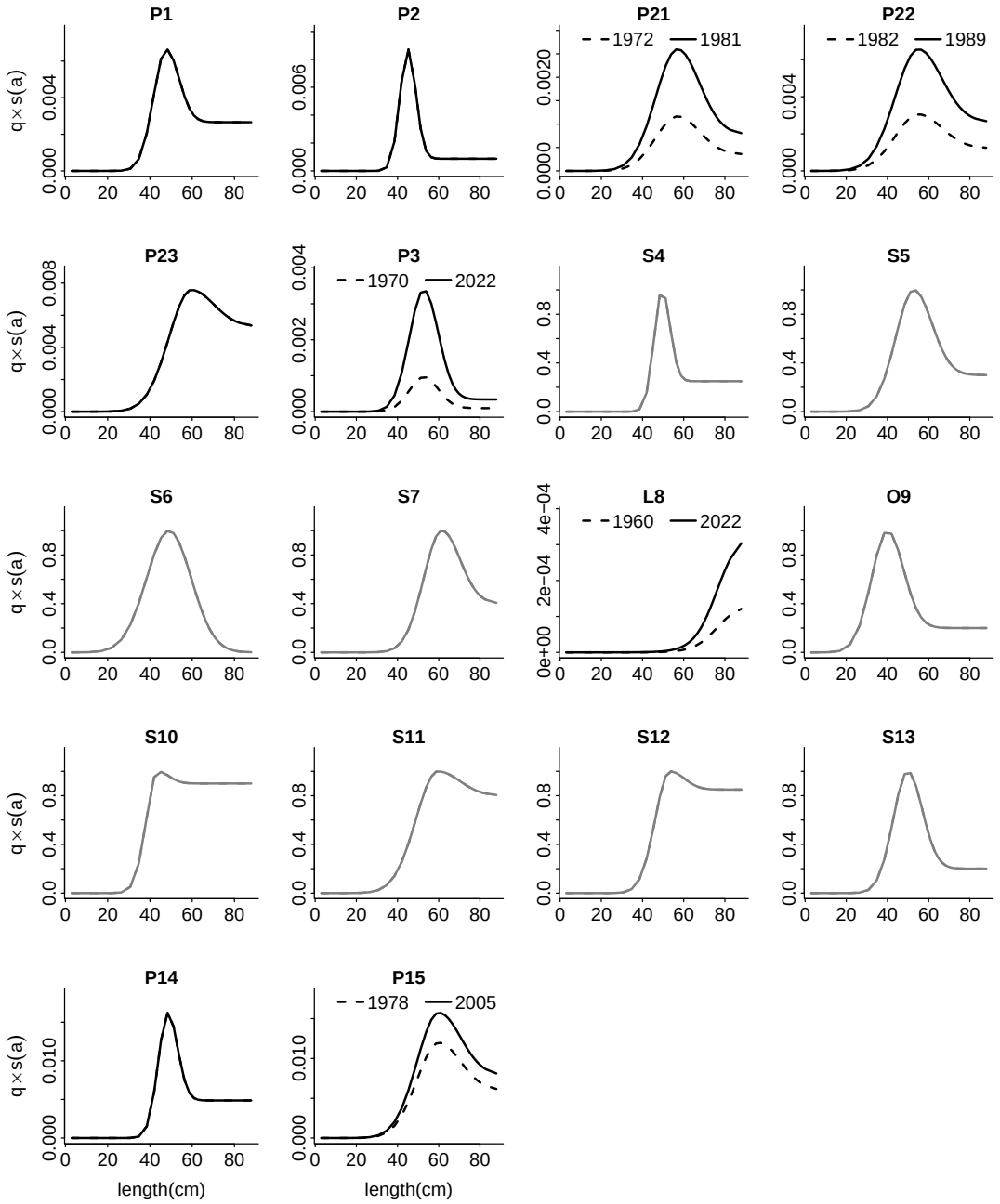

Figure 9: Catchability and selectivity by fishery in the model. The y-axis shows the product of catchability coefficient and selectivity function, which varies between 0 and 1, so that the plot gives the catchability by size. For fisheries, for which the dashed line is present, the catchability was allowed to vary linearly in time to account for the change in the gear efficiency and/or model biases. In that case the the dashed lines correspond to the catchability at size at the beginning of the run or the first year the fishery is active, and the solid lines show the catchability at size at the end of the run or at the end of the fishery's activity. Grey solid lines correspond to the catch removal fisheries, hence showing the size selectivity only.

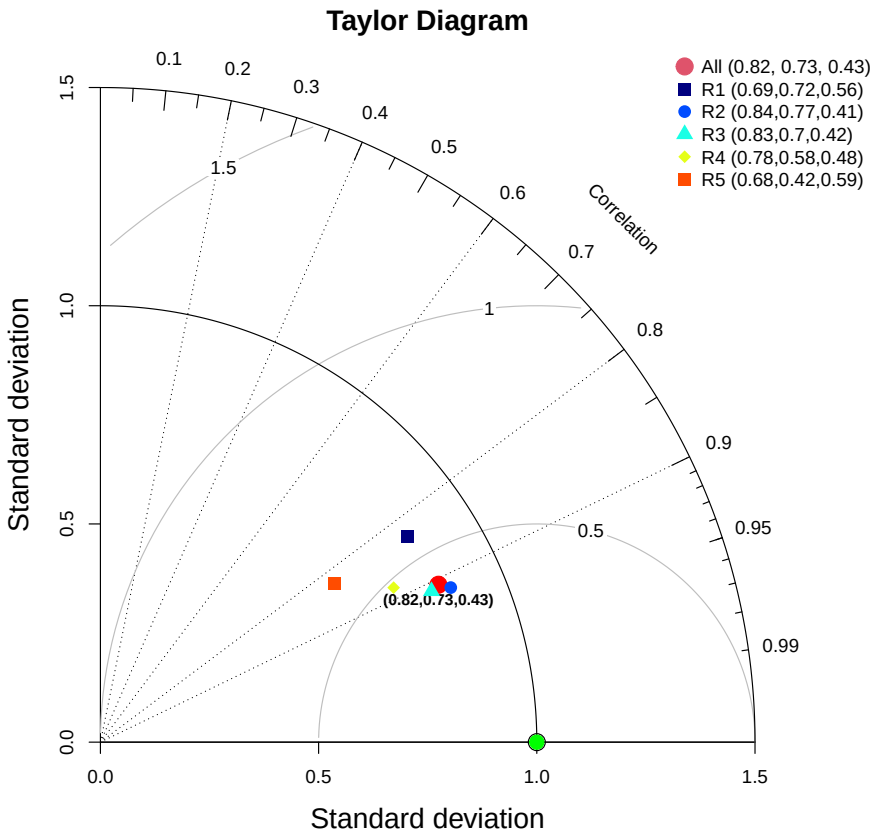

Figure 10: Taylor diagram, providing three aggregated metrics of model fit to the total catch: correlation (angular coordinates) between predictions and observations, standard deviation ratio (distance from (0,0) point depicts the ratio between model and data standard deviation) and normalized mean squared error (concentric circles with the green bullet being the center). Each point on the graph shows three metrics of the fit to the catch data by region: R1) 120E-150W, 20N-50N, R2) 140E-170E, 20S-20N, R3) 170E-150W, 20S-20N, R4) 110E-140E, 20S-20N, and R5) 150W-70W, 20S-30N. The metrics are evaluated using the catch data over 1979-2022.

Figure 11: Fit to the length frequency data over the time period of model run. Left-side distribution shows observed and right-side distributions shows predicted length frequencies. Numbers on the top of the panel correspond to NRMSE and Z-score respectively, and the number in the panel bottom shows the total annual catch, in units shown in sub-title.

a) 1979-1993 a) 1994-2005 b) 2007-2015

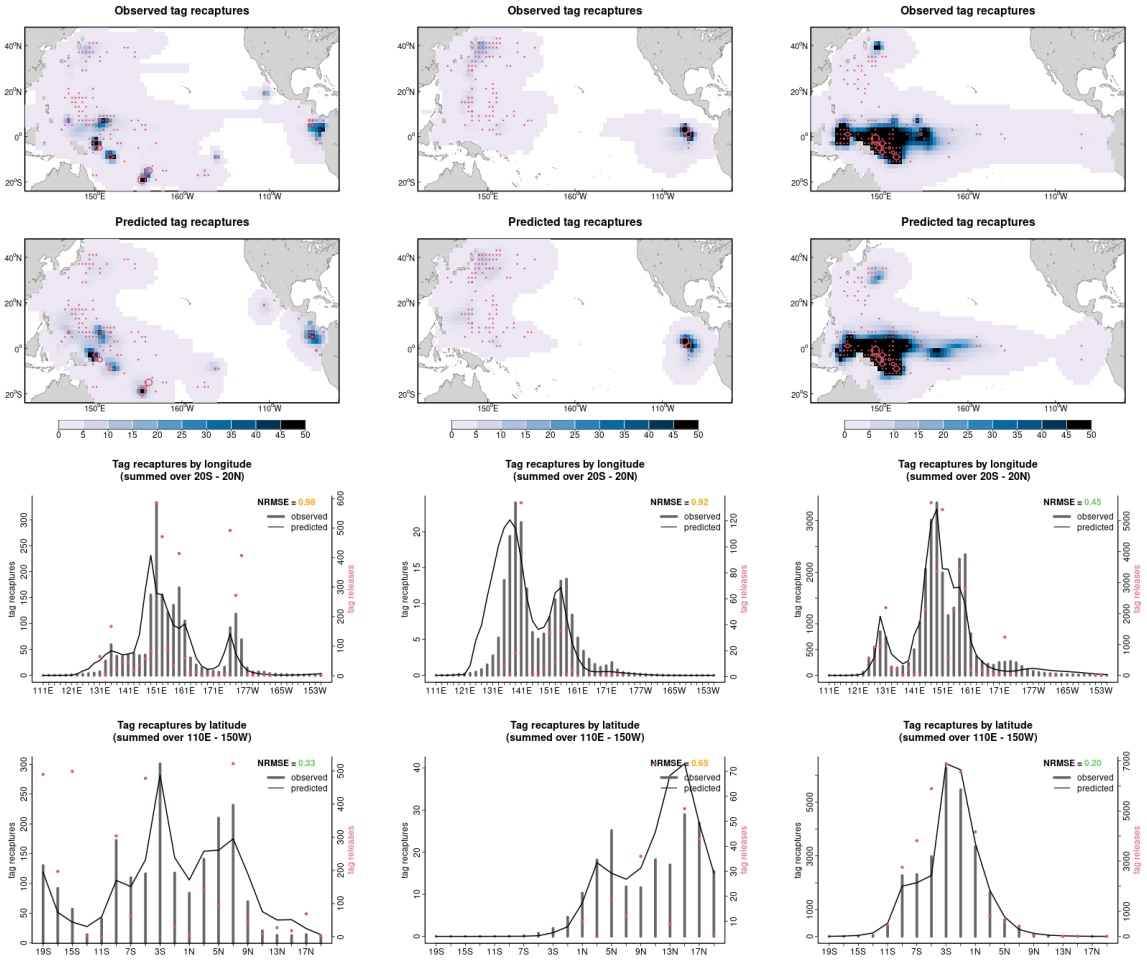

Figure 12: Maps and NRMSE metrics of fit between observed and predicted tags recaptures during different tagging campaigns. Maps show the total number of tag recaptures observed over each period, and the corresponding 1D profiles show the fit to the tropical WCPO data. Bars correspond to the number of observed tags recaptures and solid lines correspond to predicted tag recaptures.

a) 1988-1999 b) 2007 c) 2008-2010

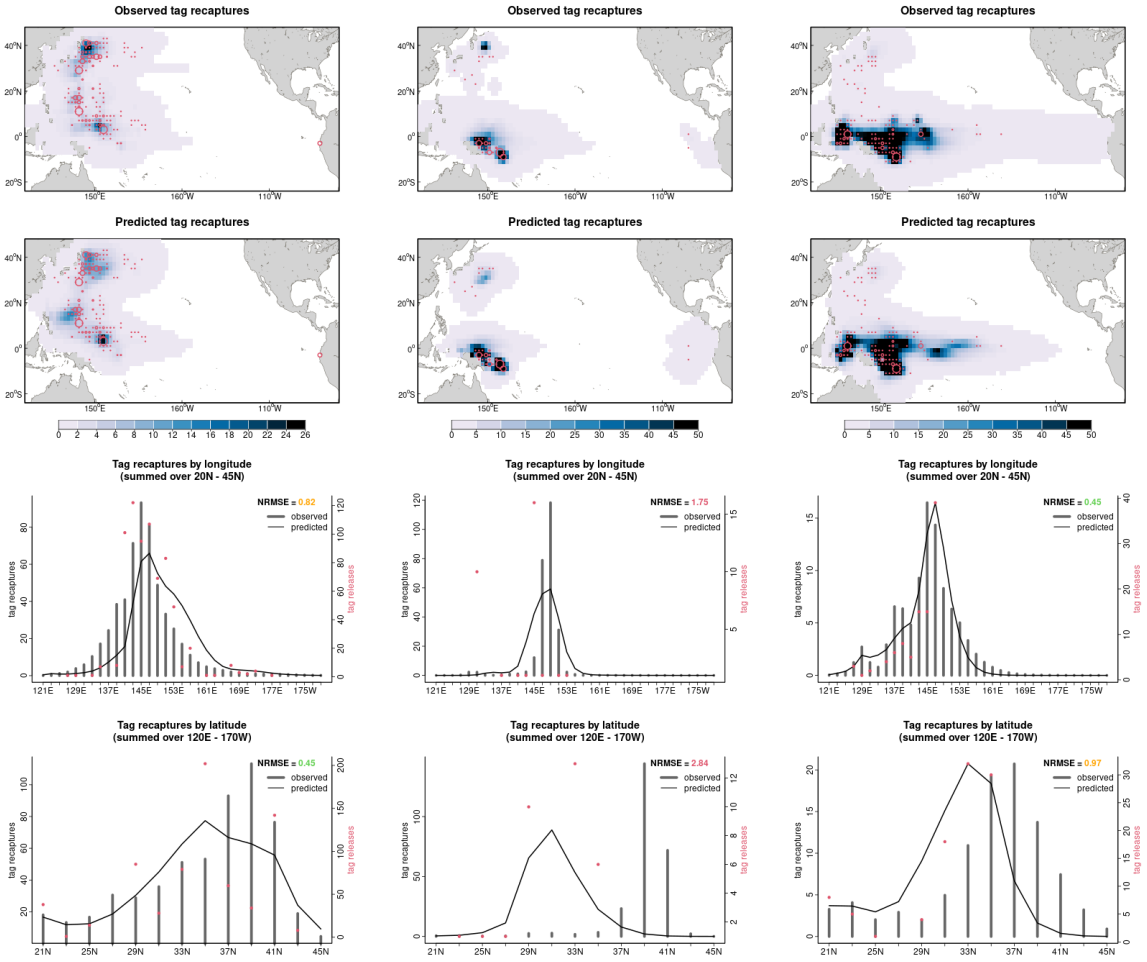

Figure 13: Maps and NRMSE metrics of fit between observed and predicted tags recaptures during different tagging campaigns. Maps show the total number of tag recaptures observed over each period, and the corresponding 1D profiles show the fit to the subtropical WCPO data. Bars correspond to the number of observed tags recaptures and solid lines correspond to predicted tag recaptures.

a) 1979-1981 b) 2000-2006 c) 2019-2022

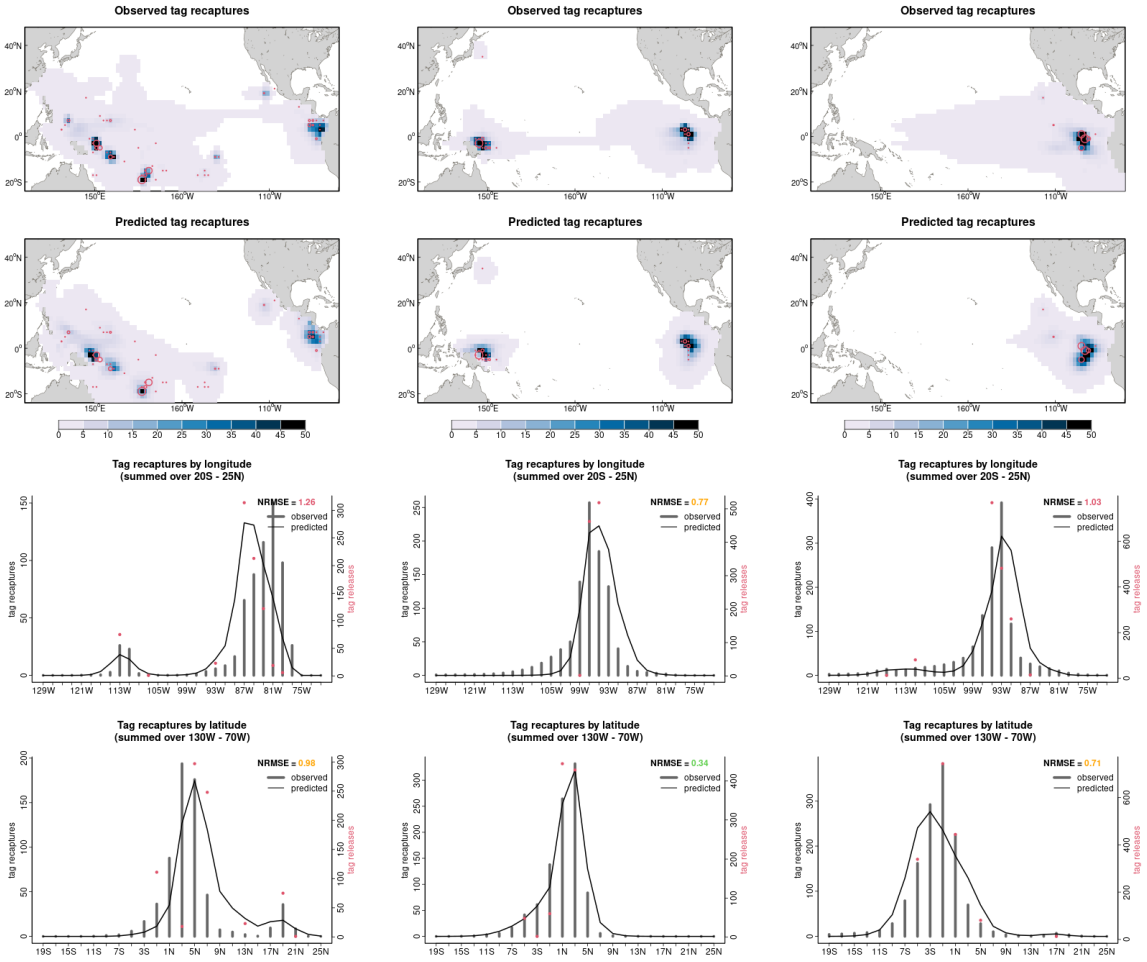

Figure 14: Maps and NRMSE metrics of fit between observed and predicted tags recaptures during different tagging campaigns. Maps show the total number of tag recaptures observed over each period, and the corresponding 1D profiles show the fit to the subtropical WCPO data. Bars correspond to the number of observed tags recaptures and solid lines correspond to predicted tag recaptures.

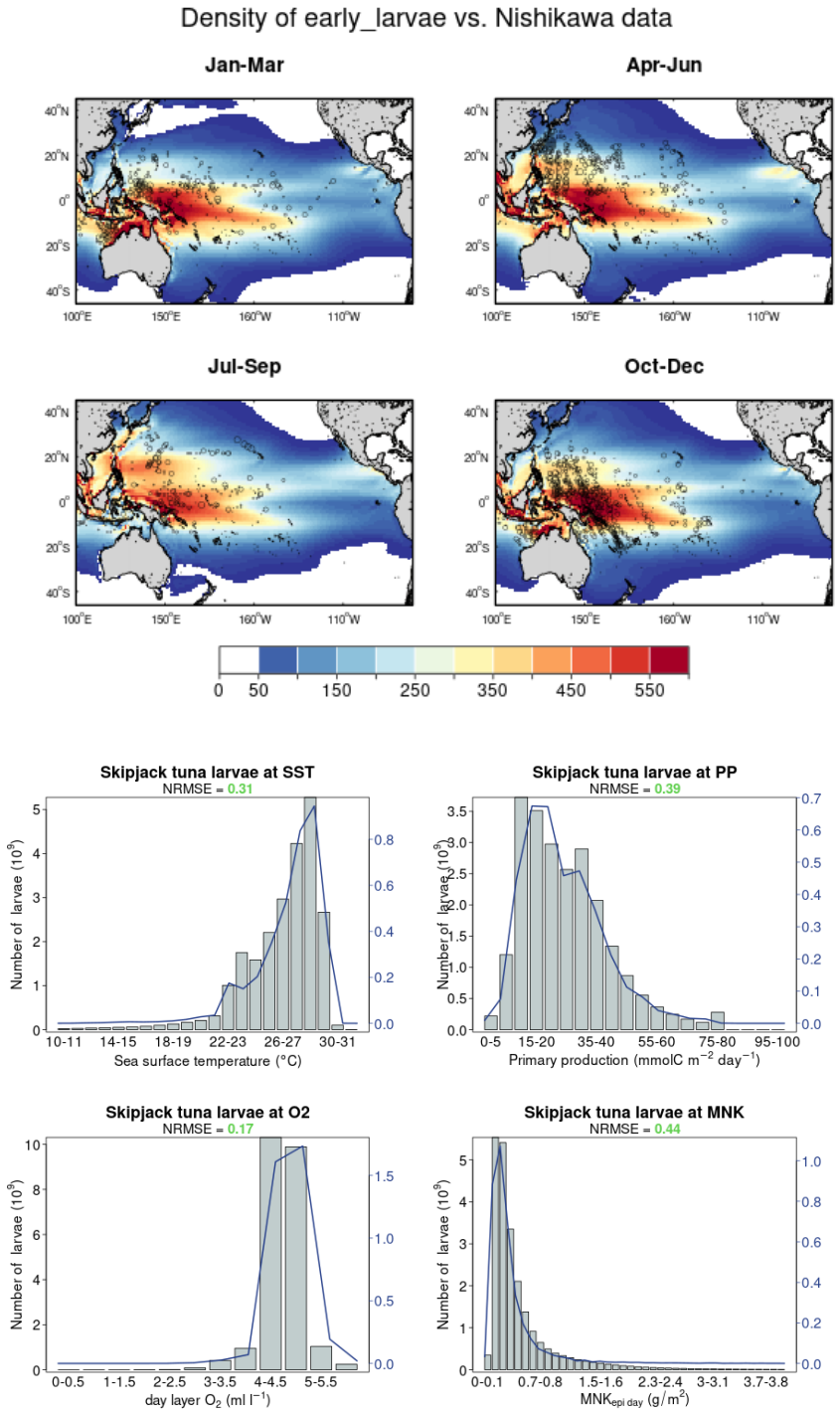

Figure 15: Validation of the early-life history data. Upper panel - seasonal spatial distributions of predicted larvae one week after spawning, with circles corresponding to the observed larval densities. The histograms on the bottom panel show the mean predicted (bars) vs. observed (solid lines) number of skipjack larvae in association with sea surface temperature, primary production, dissolved oxygen in the epipelagic layer and epipelagic forage.

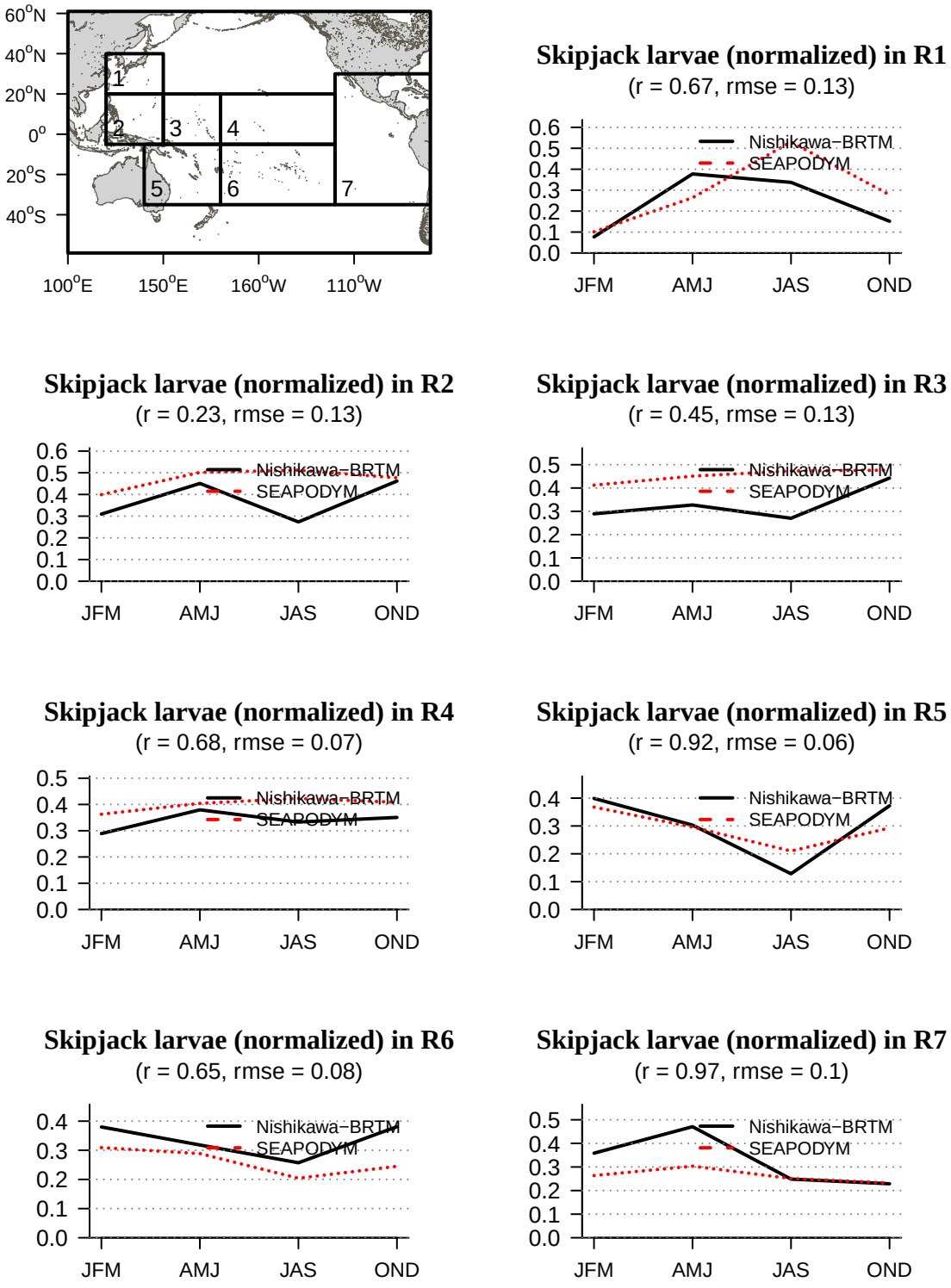

Figure 16: Seasonality of predicted normalize larval density (averaged over 1960-1981) and BRTM outputs (Buenafe *et al.*, 2025) derived from categorical larval densities (Nishikawa *et al.*, 1985).

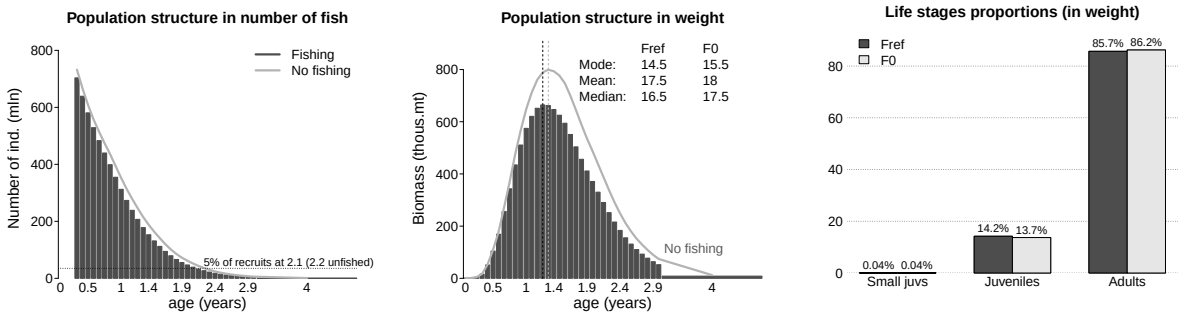

Figure 17: Population structure of Pacific skipjack tuna predicted with estimated parameters: the number and the biomass of fish by age class, and the total biomass by life stage. The light grey lines and bars correspond to the metrics of unfished population.

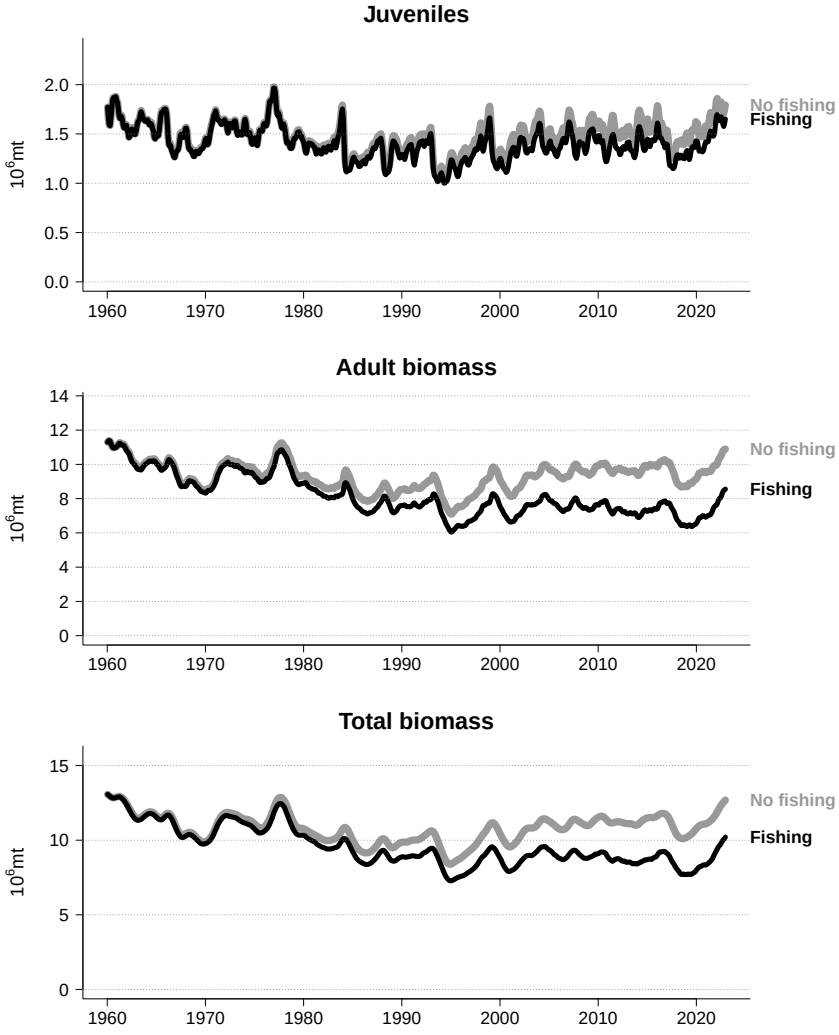

Figure 18: Predicted with estimated parameters Pacific-wide biomass of juvenile and adult skipjack tuna with and without fishing.

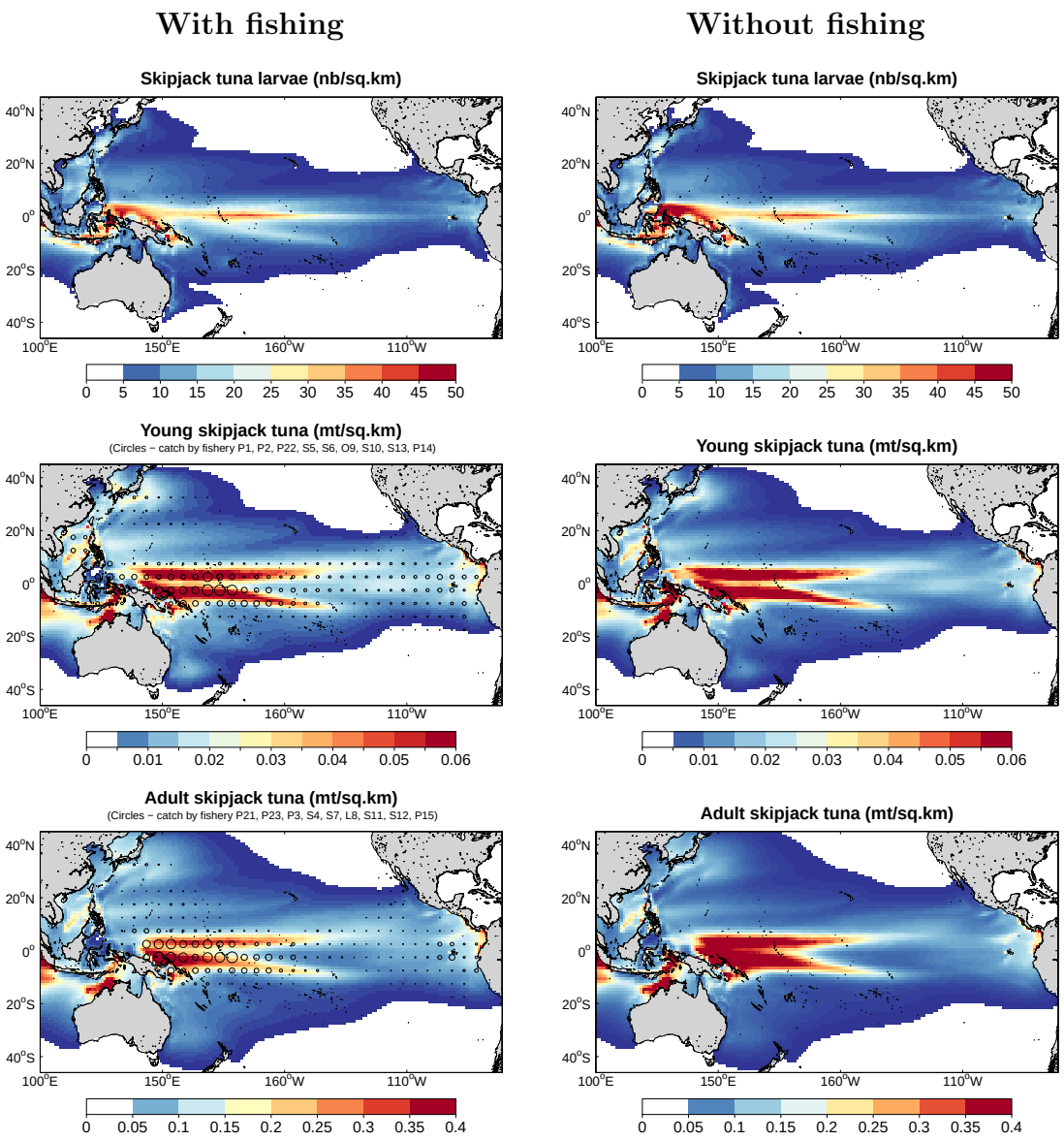

Figure 19: From top to bottom: average (over 2011-2020) density of larval (Nb/km^2), juvenile (called young, mt/km^2, including all age classes younger than age at 50% maturity) and adult (mt/km^2, including all age classes older than age at 50% maturity) skipjack tuna predicted with (left) and without fishing (right).

a) Recruits

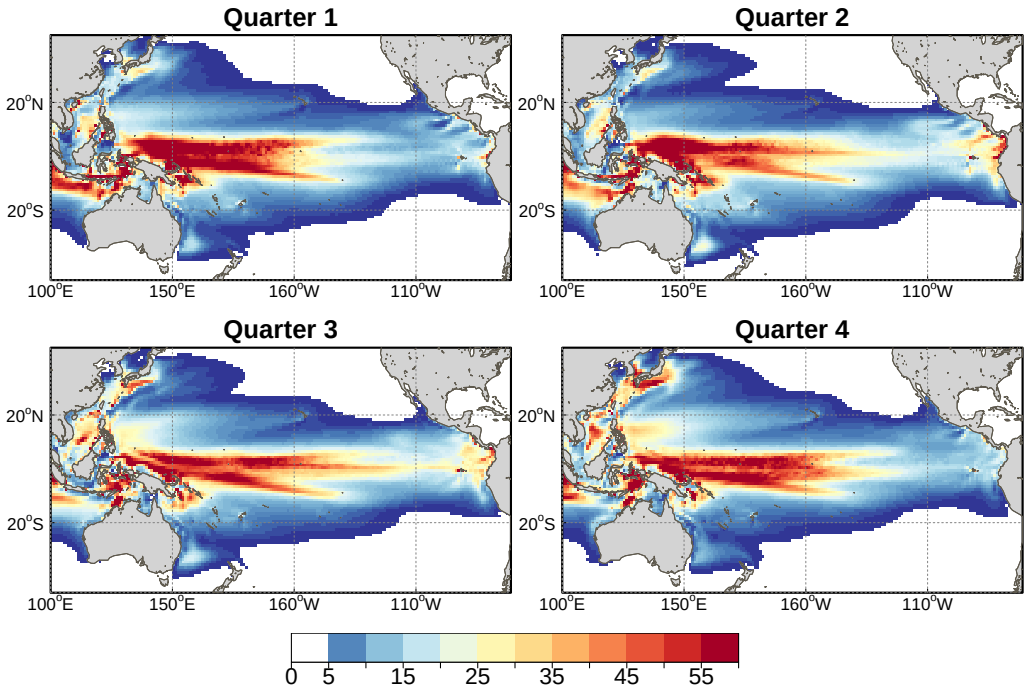

b) Adults

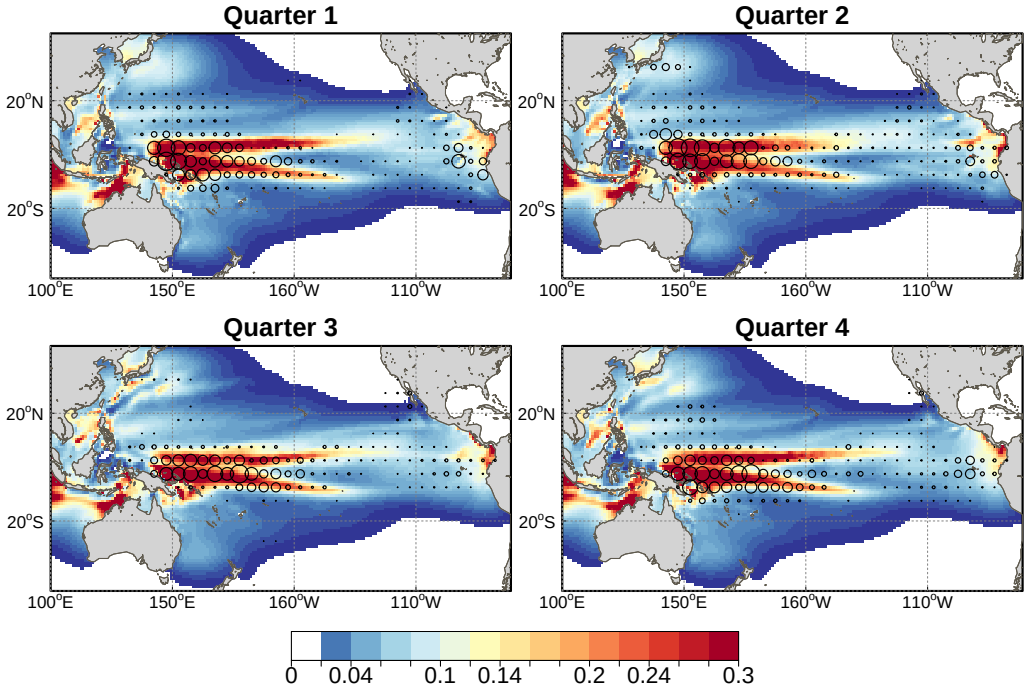

Figure 20: Seasonal distributions of skipjack tuna density at recruitment and at mature adult stage (average over 2011-2020).

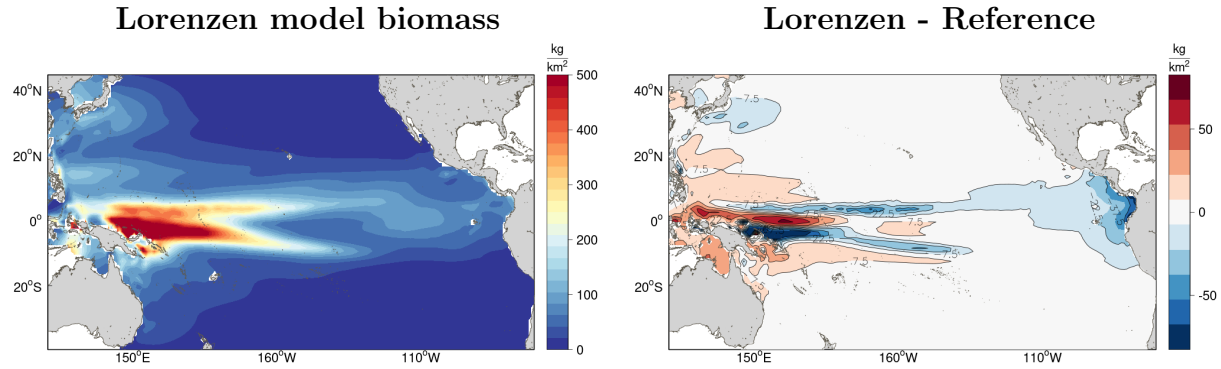

Figure 21: Spatial distribution of total (sum of juveniles and adults) biomass (kg/km^2) of skipjack tuna predicted with parameters re-estimated with fixed Lorenzen mortality and mean difference between Lorenzen-based model and reference model is calculated over decade 2001-2010.

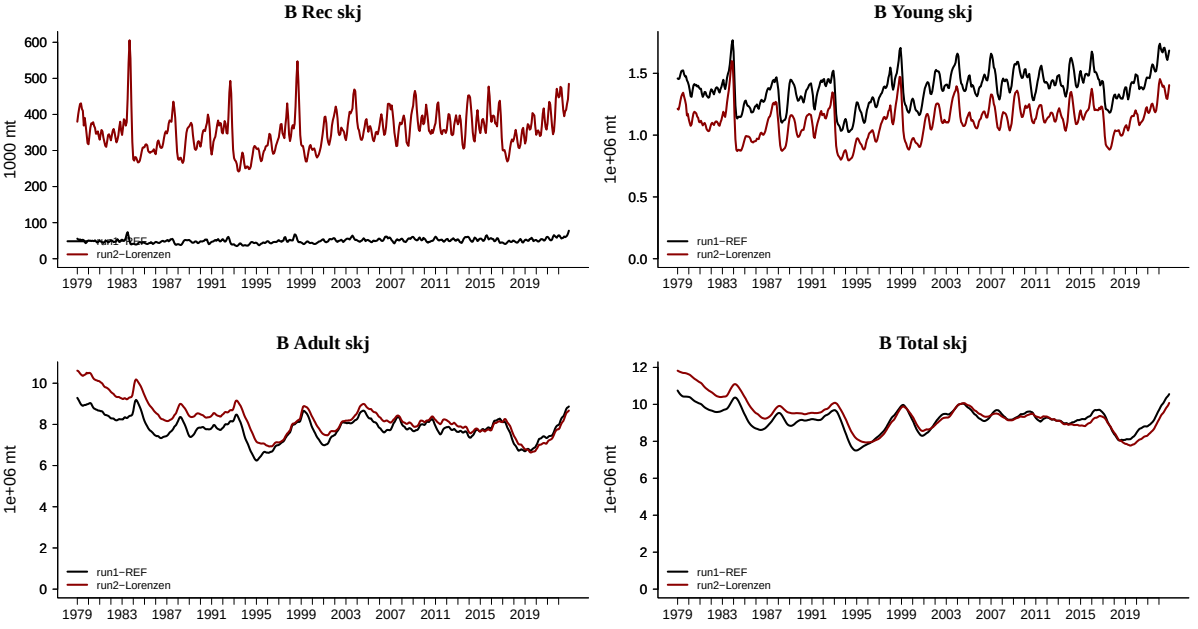

Figure 22: Comparison on SEAPODYM estimations between the reference model and the model with fixed Lorenzen mortality function.

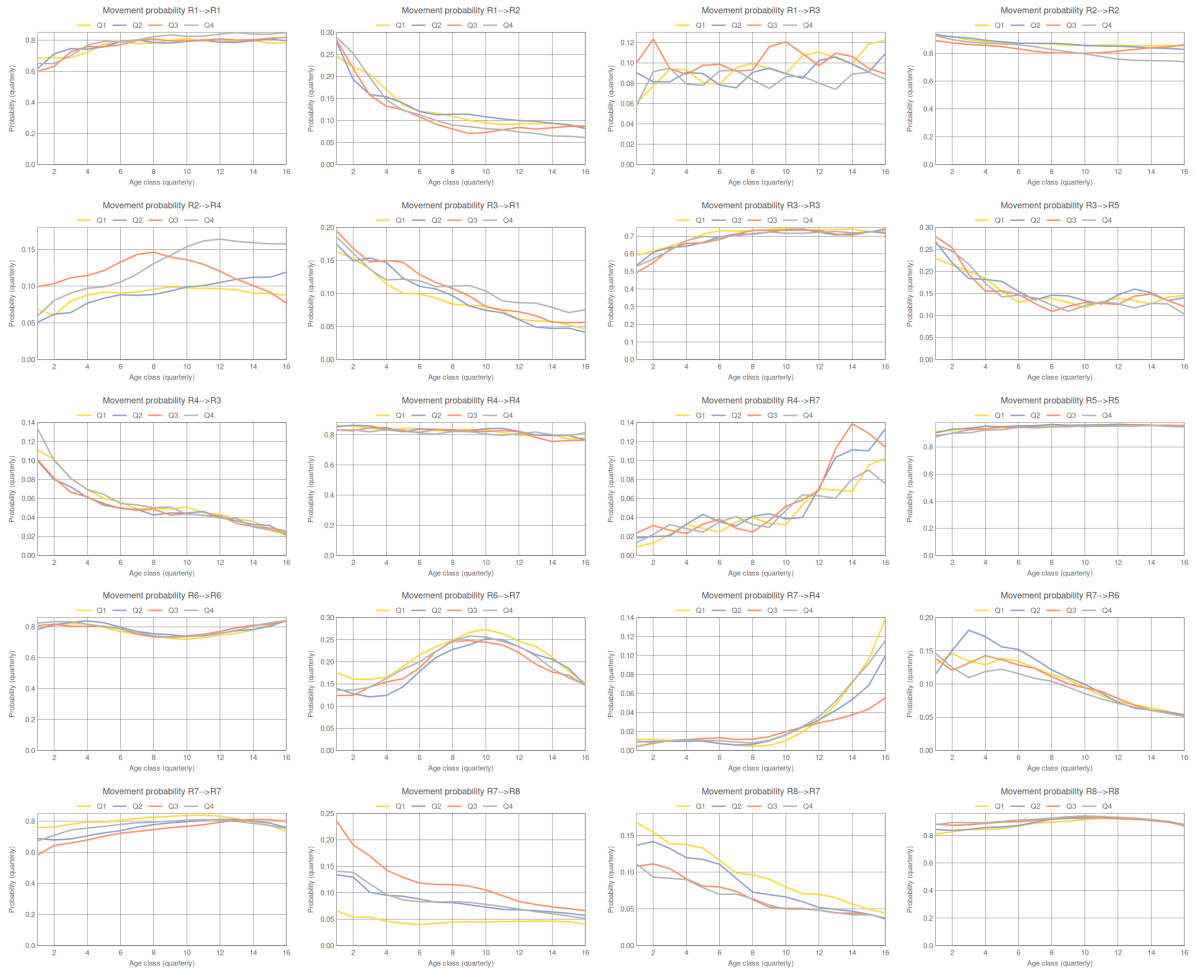

Figure 23: Regional movement probabilities. Only regions predicted to have movement probabilities greater that 0.1 per quarter are shown.

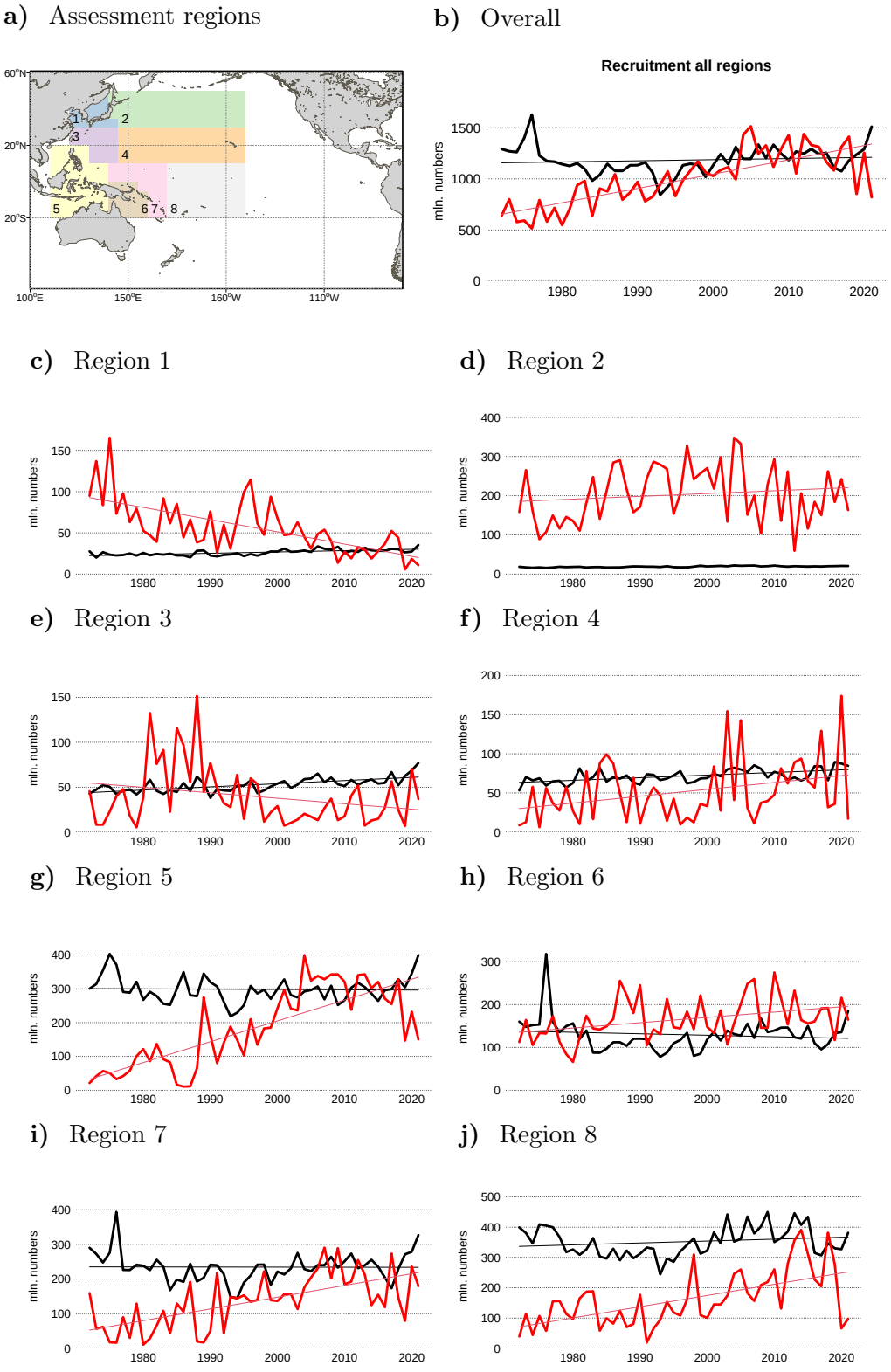

Figure 24: Comparison between SEAPODYM (black) and Multifan-CL (red) stock assessment model predictions for the Western and Central Pacific stock of recruits (mln. Nb).

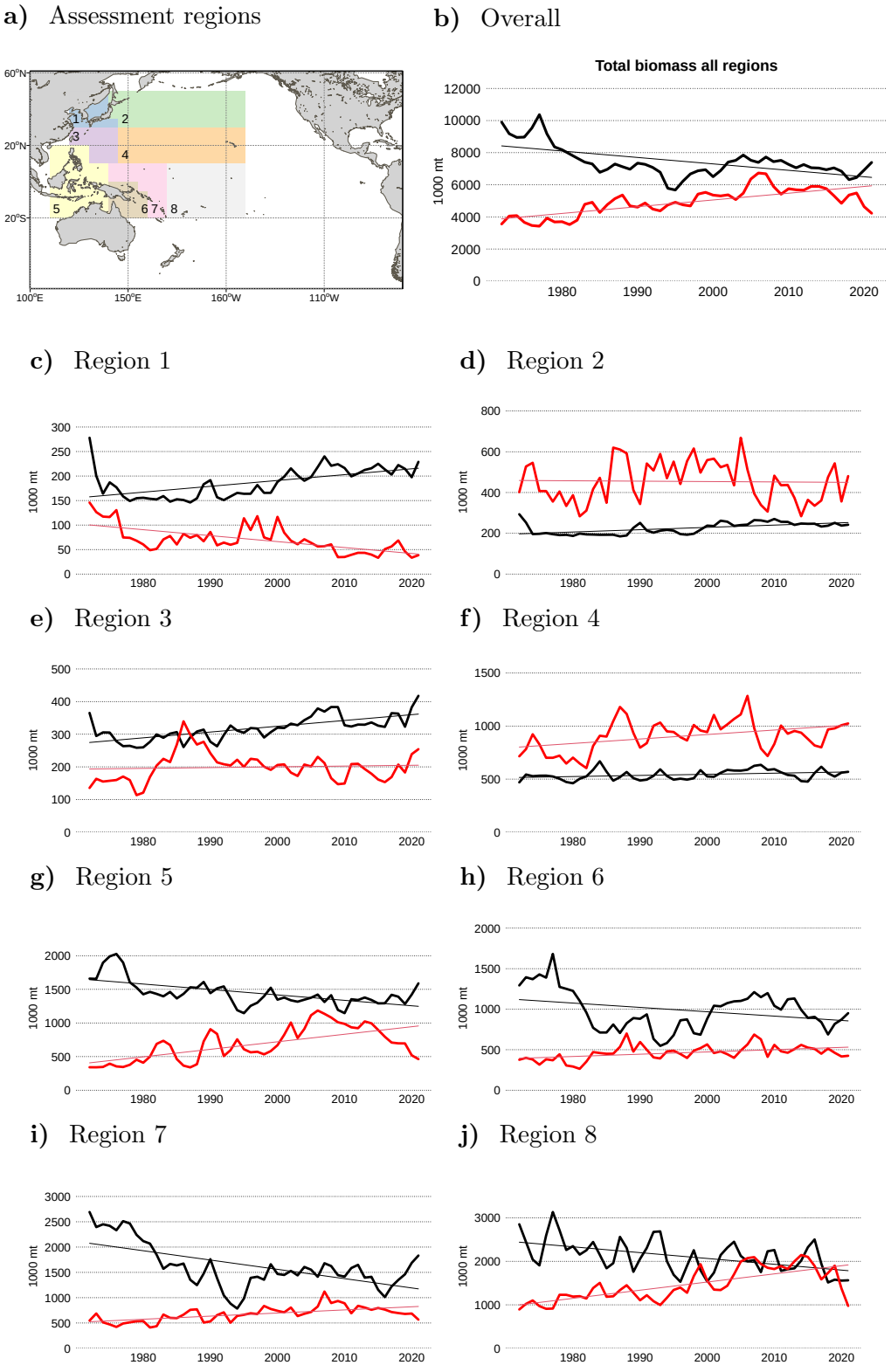

Figure 25: Comparison between SEAPODYM (black) and Multifan-CL (red) stock assessment model predictions for the Western and Central Pacific total (juveniles and adults) skipjack biomass (in thousand metric tons).

a)

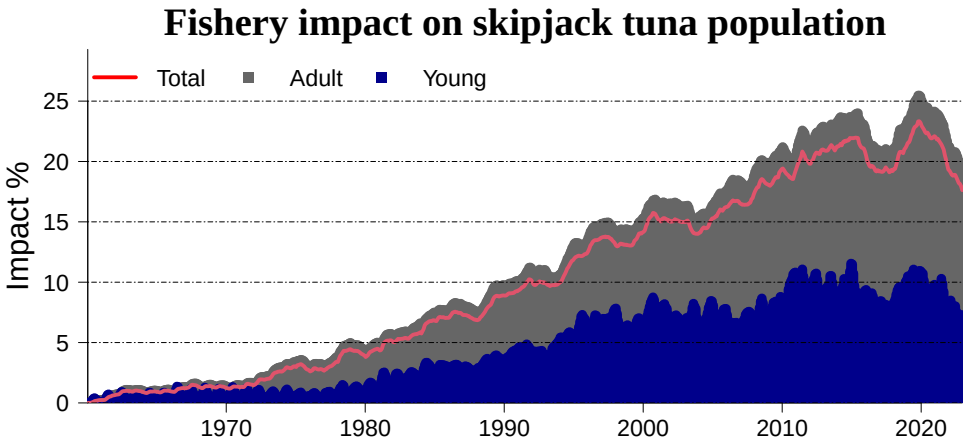

b)

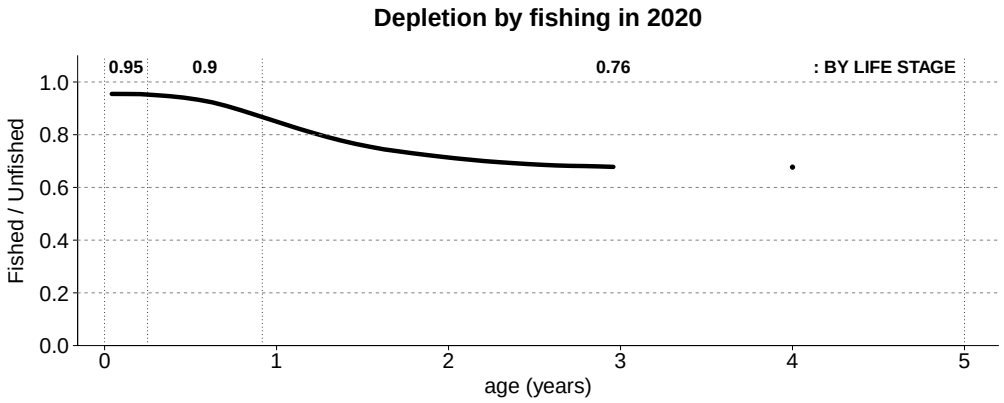

Figure 26: a) Fishing impact on skipjack population in time, calculated as $\frac{B_{F0}-B_{ref}}{B_{F0}}$. b) Fishing depletion ratio by age class calculated as a 2020 average.

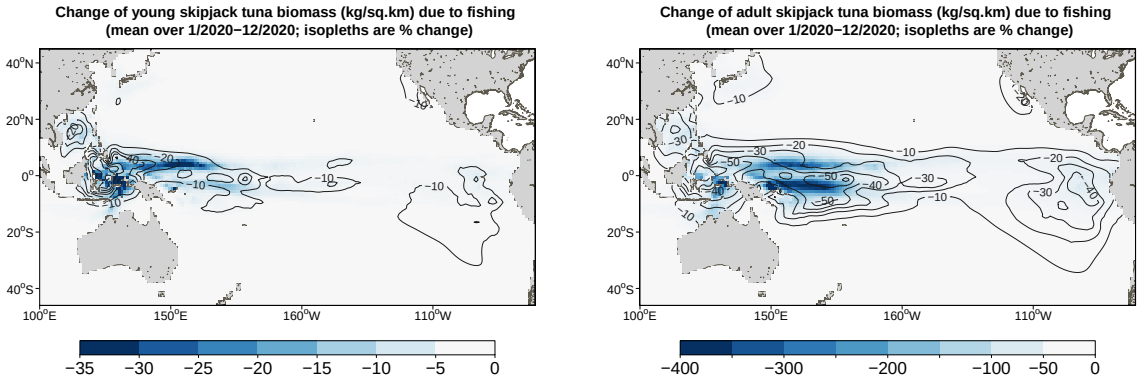

Figure 27: Spatial fishing impact on juvenile and adult population stages of skipjack in 2020. Contour lines show the index $\frac{B_{F0}-B_{ref}}{B_{F0}}$ and colour shows the average biomass reduction due to fishing.

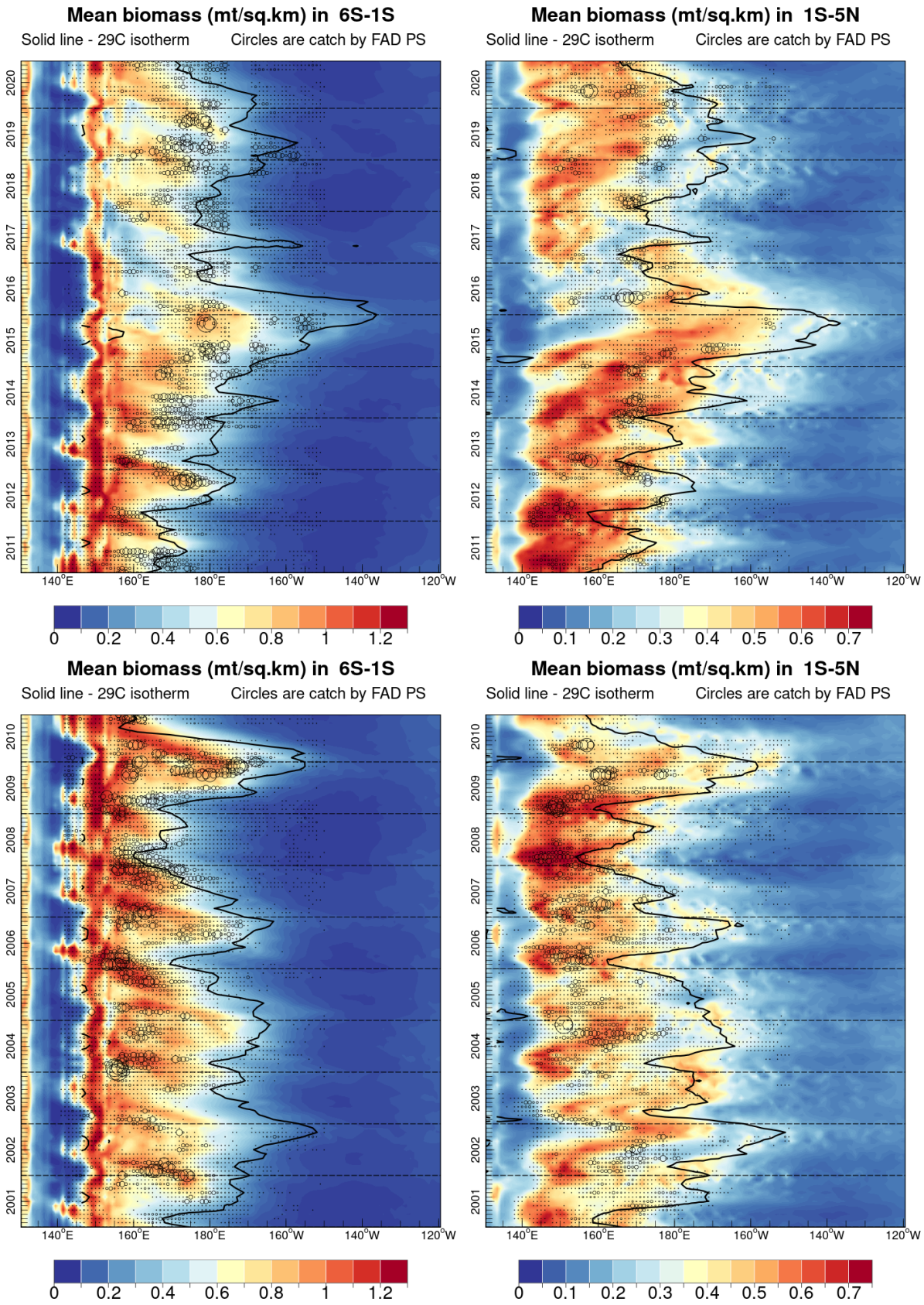

Figure 28: Hovmoller diagrams of unfished biomass. Note the different range of biomass shown due to spatial differences between south- and north-equatorial sub-stock densities.

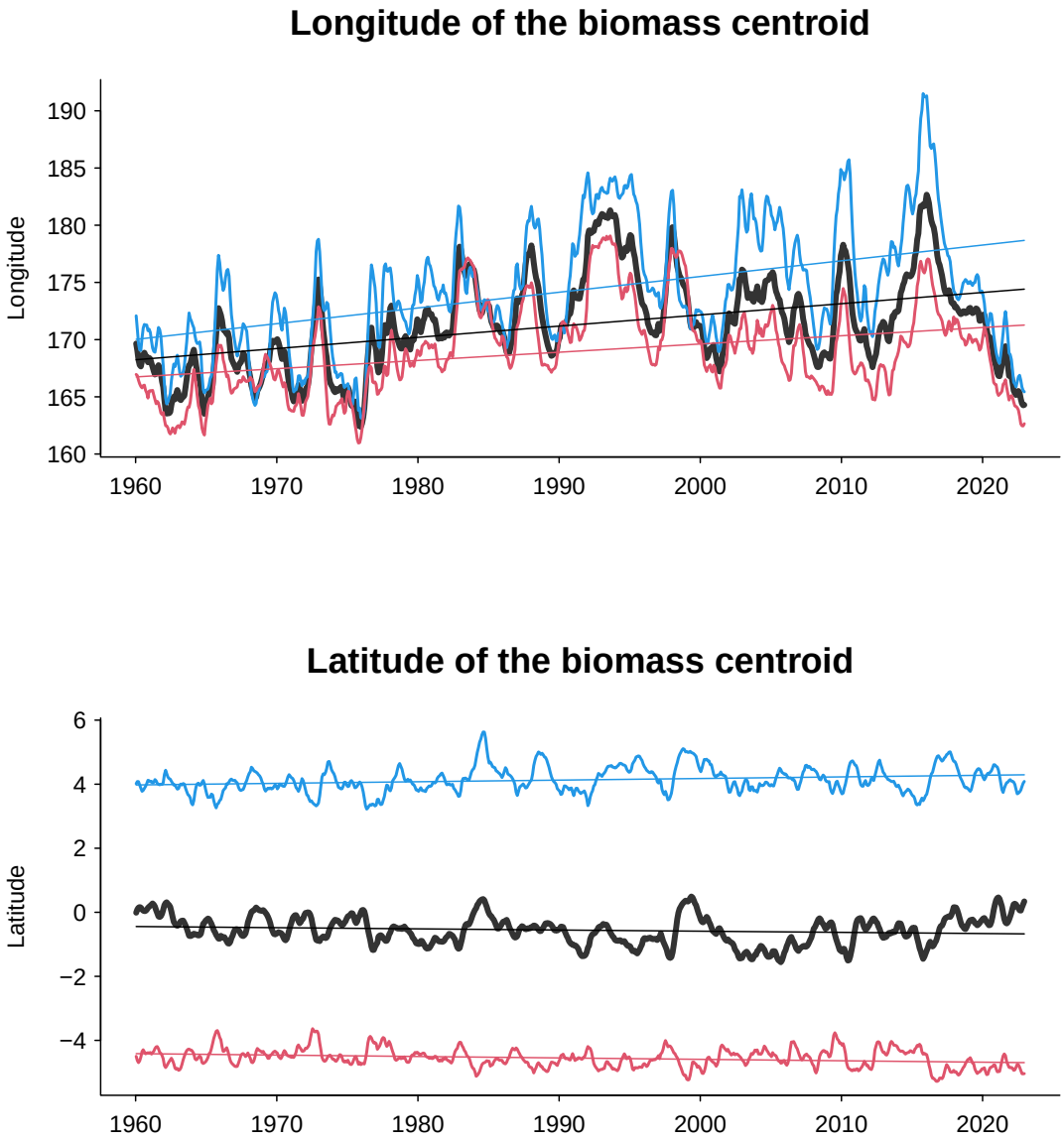

Figure 29: Total biomass centroid coordinates calculated over region 130E-130W and 10S-10N. The blue and red lines refer to the northern and southern stock respectively.

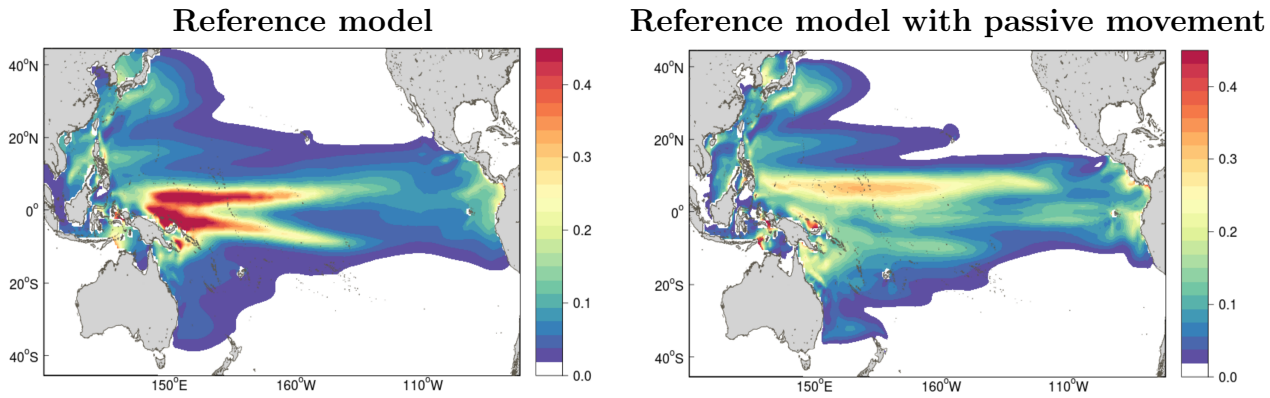

Figure 30: Spatial distributions of total (sum of juveniles and adults) biomass (kg/km^2) of skipjack tuna simulated with reference parameters (left) and with passive movement only (drift with current and small diffusive movement to account for the impact of water turbulence). Average biomass over decade 2013-2022 are shown.